https://doi.org/10.1016/j.marpetgeo.2018.06.004

Modeling lateral facies heterogeneity of an upper Oligocene carbonate ramp (Salento, southern Italy)

Laura Tomassetti*[1], Lorenzo Petracchini[2], Marco Brandano[1,2], Fabio Trippetta[1], Andrea Tomassi[1]

1. Dipartimento di Scienze della Terra, Sapienza Università di Roma, P.le Aldo Moro 5, I-00185 Rome, Italy

2. Istituto di Geologia Ambientale e Geoingegneria, Consiglio Nazionale delle Ricerche, Rome, Italy

**corresponding author*: Laura Tomassetti, email: laura.tomassetti@uniroma1.it

Abstract

The aim of this work is to reproduce a metre-scale facies heterogeneity 3D model of the Chattian Porto Badisco Calcarenite carbonate ramp outcropping in the Salento Peninsula (southern Italy). However, in shallow-water carbonate systems, capturing metre-scale facies heterogeneity in three-dimensional models remains controversial due to the possibility of facies coexistence and because their association can change through time and space.

Within this context, the continuous and well-exposed Chattian Porto Badisco Calcarenite carbonate ramp allows detailed study of the distribution of lithofacies association and their architecture along the dip direction depositional profile. The lithofacies and the depositional model of the Porto Badisco Calcarenite are referred to those defined by Pomar et al. (2014). The Porto Badisco Calcarenite is a homoclinal carbonate ramp with a euphotic inner setting characterised by the extensive seagrass meadows, passing basinward into a large rotaliid packstone and coral mounds developed in mesophotic conditions. The deeper part of the

oligophotic zone is characterised by rhodolithic floatstone to rudstone and large lepidocyclinid packstone. The distal part of the ramp is characterise by a fine calcarenite.

The methodology used in this work combines classical field data collection (e.g., stratigraphic logs and field-facies mapping) and 3D stochastic modeling by using Petrel^{TM}. All the data (top and base of stratigraphic logs, cross-section, key surfaces, lithofacies lateral extension etc.) were georeferenced and inserted into the software to build the digital outcrop model. The 3D facies model has been performed after several simulations through specific stochastic algorithms (SISim, TGSim), comparing the models reproduce by the two algorithms, matching the depositional geometries and the lithofacies association observed in the outcrop. The 3D modeling represents a useful tool to better understand the facies architecture and their complex heterogeneity. Moreover, a detailed 3D facies model provides an essential tool to characterise semi-quantitatively sedimentological features for subsurface reservoir studies.

1. Introduction

3D modeling of carbonate systems represents an important tool for the study and characterization of sub-surface reservoirs (Blendinger et al., 2004; Adams et al., 2005; Aigner et al., 2007; Qi et al., 2007; Borgomano et al., 2008; Kenter et al., 2008; Palermo et al., 2010; Tomás et al., 2010; Amour et al 2012, 2013) because carbonates currently account for 60% of the world's oil and 40% of world's gas reserves. Outcrop modeling provides the opportunity to investigate and reconstruct the depositional geometries and the physical distributions of heterogeneities in potential reservoirs (Bosence et al 1998; Warlich et al 2005; Palermo et al 2010; Tomas et al 2010). Several simulation algorithms (e.g. stochastic pixel-based, surface-based *vs.* object-based, multipoint statistics) and techniques (e.g. deterministic seismic data, well and log data) exist, and are constantly being improved (Matheron et al.; 1987; Gómez-Hermández and Srivastava, 1990;

Guardiano and Srivastava, 1993; Gringarten and Deutsch, 2001; Strebelle, 2002; Adams et al., 2005; Kenter et al., 2008; Tolosana-Delgado et al., 2008; Amour et al 2012, 2013; Janson and Madriz, 2012) to better capture the complexity of the facies heterogeneities of sedimentary systems. In facies modeling the most used technique, both for outcrop and sub-surface models, is stochastic simulation because it allows to generate multiple equiprobable realizations of a property in question (Kjonsvik et al., 1994; White et al., 2003; Falivene et al., 2007; Pöppelreiter et al., 2008; Koehrer et al*.,* 2010). Despite improvements to stochastic algorithms, the capability and geological knowledge of the modeler still play a crucial role on the final quality and reliability of the model (Journel et al 1998; Falivenne et al 2007). This is particularly true in shallow-water carbonate systems modeling because the response of carbonates to the interaction of internal and external factors is more complex due to the sensibility of carbonate-producing biota to the environmental factors and changes. Carbonate systems can display different facies arrangement from mosaic-like to regular facies belt trends (Wright and Burgess 2005). This results in a potentially high degree of facies heterogeneity. The continuous and well-exposed Chattian Porto Badisco Calcarenite carbonate ramp studied here, provides the opportunity to perform a detailed 3D model of facies association and distribution along the depositional profile, thus giving some clues to understand the high degree of facies heterogeneity in this kind of sedimentary systems. Two different stochastic modeling techniques as Truncated Gaussian Simulation (TGSim) (White et al. 2003) and the Sequential Indicator Simulation (SISim) (Matheron et al., 1987; Galli et al., 1994; Kjonsvik et al., 1994; Deutsch and Journel, 1998; Zappa et al., 2006; Aigner et al., 2007; Koehrer et al., 2010; Amour et al., 2012) were used and compare to accommodate the scale-dependent nature of geological heterogeneity. The resulting models were compared to discuss which of the two algorithms better reproduce the three dimensional lateral facies heterogeneity, even when the data input for the simulation are the same. The aim of this work is to show how the choice of

the simulation technique can produce different 3D facies heterogeneity models and to show the impact of that choice on the geological reliability of spatial facies relationships and their distribution along a depositional profile. This is done in order to show how the establishment of a suitable modeling strategy designed to capture the geological heterogeneity observed in the sedimentary record still remains a challenge for the building of a realistic 3-D geological model in carbonate systems.

2. Geological setting

Along the southern margin of the Mediterranean Tethys, several peri-Adriatic carbonate platforms were developed such as the Apulian carbonate platform, which represents the foreland of both the Apennine and the Dinaric thrust and fold belts (Bernoulli, 2001) (Fig. 1). This carbonate platform mainly comprises upper Triassic to upper Cretaceous shallow-marine carbonate deposits (Bosellini and Parente,1994); its margin is well preserved along the eastern coast of the platform in the Salento Peninsula, where Eocene to Miocene carbonate deposits are well exposed directly above a 4200 m thicked Cretaceous succession (Bosellini and Russo, 1992). The Eocene to Oligocene deposits are divided into two stratigraphic units known as the Castro Limestone (Eocene-Oligocene) and the Porto Badisco Calcarenite (upper Oligocene), that is the focus of this study. The Castro Limestone overlies, through a disconformity surface, Cretaceous substrate and discontinuous Eocene carbonate deposits. This unit is composed by coral-rich limestone with highly diversified coral assemblages and subordinate coralline red algae (Bosellini 2006) and by carbonate sediments strictly associated with a seagrass meadows environment (Tomassetti et al., 2016). The Castro Limestone unit is overlain by the Porto Badisco Calcarenite unit. The Porto Badisco Calcarenite is composed of horizontally bedded, weakly cemented, skeletal-rich calcarenite. These horizontal beds really show their depositional dip because of the absence of

faults and tectonic dip in the studied area. The entire thickness of the Porto Badisco Calcarenite unit in the Salento Peninsula is up-to 60m (Pomar et al., 2014); whereas in our studied area the Porto Badisco Calcarnite is a 35-to-40m thick. The main biogenic components are coralline red algae, forming 10-to-20-cm sized rhodoliths, and larger benthic foraminifera (LBF), and subordinated corals (Brandano et al., 2010; Pomar et al., 2014). The Porto Badisco Calcarenite is unconformably overlain by the 5- to 30-cm thick, phosphate and glauconite-rich middle Miocene "Aturia level" (Bosellini et al.,1999).

2.1. Porto Badisco carbonate ramp facies association

The facies association and depositional model of the Porto Badisco Calcarenite were previously described in detail by Pomar et al. (2014). Pomar et al. (2014) recognised six lithofacies within the Porto Badisco Calcarenite. These show a recurrent order within sub-horizontal beds and display very high heterogeneity in the dip direction In this study, we provide a brief summary of the facies association that were used for the building of the geocellular model. The lithofacies are: I) small benthic foraminifera wackestone to packstone (SG); II) coral mound (CM); III) large rotaliids packstone (LR); IV) rhodolithic floatstone to rudstone (RF); V) large lepidocyclinid packstone (LL); VI) fine bioclastic calcarenite (FC). Lithofacies associations are arranged into a homoclinal carbonate ramp (Fig. 2). This ramp is subdivided into an euphotic inner ramp dominated by small benthic foraminifera wackestone to packstone lithofacies where autochthonous biota (e.g. epyphitic foraminifera, articulated red algae) suggest the presence of well-preserved seagrass meadows. Basinward, a mesophotic to oligophotic dominated middle ramp is characterised by large rotaliids packstone and small coral mounds interfingering with rhodolithic floatstone to rudstone and large lepidocyclind packstone lithofacies. The more distal part of the ramp is characterised by a fine calcarenite lithofacies rich in fragmented skeletal debris, which was swept

from the inner to middle part of the ramp. A progressive increase in water depth occurred moving from the euphotic zone, dominated by the seagrass lithofacies, to the meso-oligophotic zone where large lepidocyclinid packstone and fine calcarenite lithofacies deposited. According to Pomar et al. (2014), the most prolific carbonate production took place in the meso to oligophotic zone, whereas the euphotic zone with seagrass-related sediments was less productive.

3. Methods

The methodology used in this work combines field data collection and 3D stochastic modeling by using PETREL™ 2016 (Schlumberger trademark).

3.1. Field data acquisition

A total of eleven stratigraphic logs were measured, nine were parallel to the depositional dip direction, along the margin of the N-S-oriented Porto Badisco ravine, and two logs were perpendicular to the depositional dip direction along the E-W oriented margin of the ravine (Fig. 3 a, b). The stratigraphic logs have been measured at different stratigraphic positions but physically correlable through a well-recognised and continuous stratigraphic surface physically recognisable in the field. The log spacing ranging between 20 m and 180 m along the two-orthogonal direction of margin of the ravine. Five detailed geological cross-sections (Fig. 4) and line-drawing photomosaics (Fig. 5) were carried out to better follow the lateral ordered trends of the lithofacies. The dimension of the study area is around 2,20 km^2, and it is orientated NNW-SSE with a dip azimuth of 110°. The sub-horizontal beds of the Porto Badisco Calcarenite show a dip azimuth of 150°. The lithofacies belts show the same orientation and dip azimuth of the area during the deposition; their lateral extension doesn't exceed 1 km. All the six lithofacies are recognizable in the study area and they can be easily mapped on photomosaics and it is enough

representative to show the high lateral lithofacies heterogeneity along the depositional profile of the low-angle carbonate ramp of the Porto Badisco Calcarenite. All the field data were georeferenced by using GPS; each data acquired a XYZ position information used to build a robust high resolution (8 m) and detailed (157014 points) Digital Elevation Model (DEM) that was later integrated to build the 3D digital model.

3.2. Modeling workflow

To build the 3D facies model of Porto Badisco outcrop two workflow steps were performed; i) creation of a geocellular model and ii) generation of the facies model. These two phases of the workflow will be described in the following paragraphs.

3.2.1. Geocellular model

In order to build up the geocelluar model, a DEM (8m of resolution) has been imported in the software PETREL™ (Schlumberger trademark) as a mesh of points and subsequently interpolated to generate the topographic surface (Fig. 6a). The geocellular model is 500 m in width and 1000 m in length, the top of the model is defined by the topography surface, whereas the bottom has been set at a 0 m a.s.l. which is close to the lowest stratigraphic log data (bottom of Log J at 1.30 m a.s.l.) and able to contain in the model the southern outcrops of the study area (Fig. 3a,b). The maximum vertical thickness of the geocellular model is 43 m. To build a realistic skeleton grid for the model, it is relevant to define appropriately the cell's size of the grid considering the size of the smallest geological object (e.g a bed thickness), which needed to be represented in the final model. The XYZ cell's dimensions must be small enough to reflect the horizontal and vertical facies variation. In order to capture these facies variability, the Z-dimension cell size should be no larger than half of the dimension of the smallest and /or thinnest geological object or feature observed

in the field (Amour et al 2012). In this work, the XY dimensions is the same as the size of the DEM resolution (8x8m). In the Z-dimension, the thinnest geological object observed is a bed about 0.40 m thick (in the rhodolithic floatstone to rudstone lithofacies), so the vertical dimension of the cell is set about 0.20 m. No faults are present in the study area and so the resulting 3D skeleton is a simple grid. Lastly, horizons, zones and layers were built to complete the gridding process and to better characterise the vertical cell-size. Generally, the horizons represent stratigraphic surfaces; in this case the horizons were coincident with the base surface at 0m a.s.l. (bottom horizon) and the DEM (top horizon). The interval between two horizons defines a zone that corresponds to a stratigraphic sequence or a lithological unit; here any unconformity or boundary surfaces have been identified, and only the Porto Badisco unit is modelled. The zone has been subsequently populated with 218-equally spaced (0.20 m) layers able to catch the facies variation of the Porto Badisco unit. The resulting 3D skeleton contains a total number of 4039976 cells, each cell has a dimension of 8 m x 8 m x 0.20 m in the X. Y and Z dimension respectively (Fig. 6b).

3.2.2. Facies modeling

To build the 3D facies model for the Porto Badisco Calcarenite ramp, the measured stratigraphic logs (Fig. 7a, Fig. 8a) and the cross-sections were georeferenced and imported into PETREL™ to provide detailed facies distribution at discrete locations in the model. Then, stratigraphic logs and cross-sections were upscaled (Fig. 7b; Fig. 8b) by assigning each lithofacies a unique code. The cells constituting the geocellular model were intersected by log and cross-section and so by each lithofacies. Stratigraphic logs and cross-sections conditioned the facies modeling, posing some restrictions to the modeling algorithms. To build a realistic and probable 3D facies model for the Porto Badisco carbonate ramp, a stochastic approach was followed because it is the most suitable method to reproduce the high heterogeneity in carbonate systems (Falivene et al., 2006) allowing

a (conditional) probabilistic facies analysis when hard data are not enough to capture the detailed facies distribution. Two different pixel-based algorithms were applied: the TGSim and the SISim. These two algorithms are the most used algorithms for facies modeling with PETREL ™ (Journel et al., 1998; Falivene et al., 2006; Amour et al., 2012). The modeling process was iterative to create a facies model that matches with the field geological interpretations or that is comparable with a similar geological analogue. To reproduce the high facies heterogeneity of carbonate systems, some geostatistical parameters must be considered. The first parameter is the vertical distribution of facies in the study area for each section or logs for each zone to be modelled; this is a 1D-parameter and generally reflects the real vertical distribution (or real stratigraphic thickness) in the study area. The second geostatistical parameter derives from the semi-variograms used to define the horizontal and vertical geological distribution of the object that must be modelled. The semi-variogram is a 3D parameter that conditions the facies modeling into three dimensions and it can be generated by the software elaboration or derived from geological analogue. In this work, the vertical and horizontal dimensions of lithofacies distribution was taken directly from the field outcrop; consequently, here, no semi-variograms have been used. The vertical proportion matches with the real vertical thickness of the lithofacies measured along the stratigraphic sections.

4. Results

Modeling the carbonate facies heterogeneity is not a straightforward process either at the facies association scale and or at the lithofacies scale. In this work, a stochastic approach has been used because of the necessity to reproduce the lateral ordered transitions between the lithofacies association in a dip direction from the inner ramp to the outer ramp depositional environment. This has been done using two different stochastic algorithms, the TGSim and the SISim, and then

comparing the models reproducing by each of these. In the following paragraphs, firstly, a field lithofacies analysis was given and then the description of the two algorithms.

4.1. Field facies analysis

Six lithofacies can be recognized in the Porto Badisco Calcarenite unit: small benthic foraminifer wackestone-packstone (SG), coral mounds (CM), large rotalid packstone (LR), rhodolithic floatstone (RF), large lepidocyclinid packstone (LL) and fine calcarenite (FC).

Small benthic foraminifer wackestone-packstone (SG)

This lithofacies is characterized by tabular beds, few decameters thick, consisting of small benthic foraminifer wackestone-packstone, showing a lateral extension that doesn't exceed 300 m in length and almost 15 m in height. The skeletal fraction is dominated by foraminifers including large rotalids such as *Heterostegina* and *Spiroclypeus,* small rotalids, small and large porcellaneous (*Astrotrillina* and *Peneroplis*) and encrusting foraminifers (Fig. 9a). Other abundant components are encrusting red algae fragments, while subordinate components are fragments of bryozoan and articulated red algae. Coral fragments, often encrusted by foraminifers and red algae also occur. On the basis of compositional and textural characters Pomar et al 2014 interpreted this lithofacies as produced and accumulated in a seagrass environment.

Coral mounds (CM)

The coral mounds lithofacies is associated with the seagrass meadow deposits (SG). The mounds are up to 2-3-m thick and 3- to 20-m in length. The coral colonies are mostly in living position, but some large overturned colonies are common. The growth form ranges from

domal to platy rarely is encrusting. Most colonies are in contact, but enclosed in floatstone/packstone matrix. The matrix consists of a skeletal debris represented by non-articulate red algal fragments, small benthic foraminifers (rotalids and miliolids) (Fig. 9b) and small fragments of large foraminifers (nummulitids and lepidocyclinids). Echinoid fragments are abundant. Fragments of bryozoans, brachiopods, bivalves and articulate red algae also occur. The mound structure corresponds to the cluster reef (*sensu* Riding, 2002). Corals built small and discrete mounds with inter coral spaces infilled by bioclastic matrix. The abundance of small benthic foraminifers, many of them derived from seagrass meadows, evidences transport processes from shallower settings. Mound flanks are characterized, by coral fragments. Nummulitids and *Nephrolepidina* represent autochthonous/parautochthonous components that lived in meso-oligophotic conditions, reworked and broken by episodic currents and/or storms (Pomar et al. 2014).

Large rotalid packstone (LR)

The large rotalid packstone to wackestone-packstone is dominated by fragments and reworked *Neorotalia* and *Neorotalia viennoti* (Fig. 9c). Large porcellaneous (mostly *Austrotrillina* and *Peneroplis*) are frequent. Small benthic taxa include abundant miliolids, frequent cibicidids (e.g. *Lobatula*) and some acervulinids and nubeculariids. Nummulitid fragments (mostly *Operculina* and *Heterostegina*) are abundant, while *Nephrolepidina* and *Amphistegina* are rare. Coralline algae are represented mainly by fragments of melobesioids, mastophoroids and sporolithaceans. Other skeletal components are fragments of echinoderms, bryozoans, bivalves and corals. This lithofacies occasionally shows planar crossbeds that are 10–40 cm thick. In these beds, ghost of lamination may be observed, in this case lamination forms angles of 5–10° with bedding. Its lateral dimension is around 200 m

length and 20 m in height. This lithofacies is characterized by a mixing of autochthonous meso-oligophotic components (nummulitids and *Nephrolepidina*) and allochthonous shallow euphotic elements (*Neorotalia,* thick *Amphistegina, Austrotrillina, Peneroplis,* small miliolids). Poor-preservation and fragmentation of *Neorotalia* tests is indicative of high hydrodynamic energy and intense transport processes are also implied by the mixing of seagrass-meadows components (large porcellaneous and epiphytic foraminifers) and other shallow-water components (thick *Amphistegina* tests and articulate red algae) with autochthonous large rotalids and coral fragments (Pomar et al. 2014).

Rhodolithic floatstone (RF)

The rhodolithic floatstone (RF), locally rudstone, is laterally associated with the large rotalid packstone lithofacies. Its lateral extension doesn't exceed 800 m (length) and 25 m in height. Rhodoliths are mainly laminar with bryozoan and/or acervulinids in the nuclei (Fig. 9d). Rhodolith are dispersed in a packstone matrix made up of abundant large rotalids, including reworked tests of nummulitids, *Neorotalia*, lepidocyclinids (both *Nephrolepidina* and *Eulepidina*) and thick *Amphistegina* specimens. Rare *Miogypsinoides* may occur, while. porcellaneous foraminifers are rare. Other skeletal components are represented by bryozoans and echinoid fragments, and rare bivalve, and articulate coralline algae fragments. This lithofacies is characterized by large-scale planar cross bedding with massive beds up to 2 m thick. This lithofacies represents the sedimentation in the middle ramp environment in the oligophotic zone where coralline algae rhodoliths became more abundant. Shedding of sediment from the shallow inner ramp is recorded by the occurrence of shallow-water components mostly corresponding to seagrass-associated biota. The foraminiferal association,

characterized by the occurrence of *in-situ* thin and flat *Eulepidina* specimens also confirm the depth increasing (Pomar et al. 2014).

Large lepidocyclinid packstone (LL)

The large lepidocyclinid packstone (LL) form lenticular up to 1 m thick beds dominated by abundant *Eulepidina* specimens (Fig. 9e), with a lateral extension that doesn't exceed 500 m and maximum 5m in height. Nummulitids, together well-preserved *Amphistegina*, *Neorotalia* and *Nephrolepidina* are common. The foraminiferal assemblage is also characterized by encrusting forms such as victoriellids and acervulinids. Small benthic foraminifers include discorbids, rosalinids, cibicidids, miliolids and scarcer bolivinids and textularids. Planktonic foraminifers are abundant. Components other than foraminifers include abundant non-articulate coralline algae, forming laminar rhodoliths. Bryozoan fragments are frequent, and fragments of bryozoans, bivalves and articulate red algae are rare. Classically large and flat *Eulepidina* thrived in the deeper part of the oligophotic zone, downdip of rhodolithic pavements (c.f. Buxton and Pedley, 1989; Brandano et al 2009a,b; Pomar et al 2014), in association with nummulitids and *Nephrolepidina.* The abundance of planktonic taxa is in agreement with deeper conditions. Seagrass components (thick *Amphistegina* and *Neorotalia*, small miliolids, discorbids-rosalinids and cibicidids) swept from shallow-water settings also occur in this facies belt.

Fine calcarenite (FC)

The fine calcarenite (up to 200 m in length and 2 m in height) is represented by homogeneous lenticular beds of a fine-grained bioclastic packstone to wackestone. The sediment is well-sorted and made up of highly abraded biogenic components, dominated by coralline algal debris, echinoid fragments, small benthic foraminifers and rare nummulitids and

lepidocyclinids (Fig. 9f). The fine calcarenite facies represents accumulation of the fine and well sorted bioclastic sediments shed off from the shallower inner and middle ramp environments in a zone with very scarce carbonate production placed in the aphotic zone (Pomar et al. 2014).

4.2. Truncated Gaussian Simulation (TGSim) modeling

The TGSim is a stochastic algorithm that allows the consctrucion of 3D facies models reproducing facies order transitions and so the facies heterogeneity following the rules of the Walther's law (Matheron et al., 1987). TGSim allows to replicate and to model the lithofacies variability trends throughout the Porto Badisco carbonate ramp using some constraining tools (measured stratigraphic logs and the cross-sections). A quality control-check after the running of the TGSim, shows that the geological data collected in the field are not strongly modified during their input into the model. This check consists of a visual comparison between the field measured logs with the "pseudo-logs" created by the model (Fig. 7b; Fig. 8b). This comparison demonstrates that the input data and modelled data are quite similar regardless of the thickness of the modelled beds (Fig. 7b). For example, the 3m-thick- interval of LR lithofacies in the log C is correctly modelled in the cells, as well as the smallest bed (0.20cm-thick) of the LL lithofacies in the log A is quite similar (Fig. 7b). Similarities are also observed between the geological cross-sections and those modelled by the software (Fig. 10), in which the thickness and lateral relationships of the lithofacies are respected. As shown in Fig. 11(a,b,c) is possible to recognised and compare the facies belt of the Porto Badisco Calcarenite as described by Pomar et al. (2014). For example, the SG lithofacies interfingering with the CM and LR in the inner ramp environment and moving towards the southern sector, with the RF lithofacies; whereas the middle ramp of the model is occupy by the RF lithofacies that passes towards south to the LL and FC lithofacies. This facies belt arrangement

is the same recognisable also in the field and in the photomosaics line drawing (see Fig. 5), showing that the lateral lithofacies distribution is correctly modelled.

4.3. Sequential Indicator Simulation (SISim) modeling

SISim is a stochastic algorithm based on the indicator approach that works with categorical variables like facies (Deutsch and Journel, 1998). SISim transforms each facies into a new variable and the value of the newly created variable corresponds to the probability of finding them at a particular position in the model (Falivene et al., 2007). Each facies value generated with SISim is sequentially assigned to each grid cell that populates the 3D grid without following any facies trend or order. Consequently, the SISim is not the best tool to replicate the lateral and/or vertical facies heterogeneity following Walther's law because it does not reproduce ordered facies transition. In this work, as shown in Fig. 12(a-c) the resulting 3D facies model with SISim for the Porto Badisco carbonate ramp has a patchy and random appearance even when the input data is the same used for the TGSim. In fact, only the hard data are the same of that obtained with the TGSim, while the upscaling process shows a high degree of randomness and a poor fit when comparing lateral facies transitions (Fig. 12b,c). This is true also comparing the facies belt recognised in the field and in the depositional model proposed by Pomar et al. (2014), with the ones reproduce by the SISim model. For example in the SISim, the SG lithofacies occur randomly from the inner to outer sector of the ramp, whereas in the field are just located in the more inner sector of the Porto Badisco ravine (see Fig. 1 for location and Fig. 5), and the same story happened looking lithofacies RF, LL and FC, that in the filed occur at the middle-to- outer ramp, inferring an oligophotic to aphotic zone, that occur also in the euphotic inner ramp in the model reproduce by the SISim.

5. Discussion

5.1. *Facies model* vs *outcrop model using TGSim and SISim*

The resulting 3D facies model reproduces the lateral and spatial distribution of the lithofacies association of the Porto Badisco ramp that are visible in outcrop. To test the robustness of the model, a comparison between the facies distribution in the outcrop and the facies distribution reproduced by the model was carried out. As shown in Fig. 11, is possible to recognised in the TGSim-based model the six recognised lithofacies, with the corresponding depositional environments of the Chattian Porto Badisco carbonate ramp. Looking at the depositional model (Fig. 2), the facies belt are arranged, moving from inner sector (north) to outer sector (south) with the seagrass lithofacies (SG), dominated the euphotic zone, interfingering with the large rotaliid (LR) and the coral mound (CM) lithofacies in the euphotic to mesophotic zone, and subsequently with the rhodolithic floatstone (RF) lithofacies in the oligophotic zone. The middle-outer sectors of the ramp are occupied by the lepidocyclinids packstone (LL) and the fine calcarenite (FC) lithofacies. Looking at the 3D model produce by the TGSim (Fig 11a-c), this order is replicated throughout the ramp, for example the mesophotic CM lithofacies (in red) occur in front of (seaward) the SG lithofacies (in green), laterally interfingering with the SG and LR (in yellow) lithofacies (Fig. 11b), showing also some interfingering with the RF (in purple) lithofacies towards the south direction (middle ramp sector) (Fig. 11c) reflecting the N-S orientation of the facies belt for the Porto Badisco carbonate ramp consistent with the model proposed by Pomar et al., (2014). In the field, the CM lithofacies is characterised by a typical mound-like structure with convex morphology and well-defined flanks. Looking at the model produced by TGSim, this geometry is quite well-reproduced and the CM lithofacies appears as 3D red lenses embedded within the green SG lithofacies and yellow LR lithofacies (Fig. 11; Fig. 13), reproducing once again the fidelity with the model of Pomar et al. 2014 (Fig. 2). Looking at the model generated by the SISim (Fig. 12a- c) this association is not reproduced as well as the lateral interfingering between the SG, LR

and CM lithofacies in the inner ramp setting. A similar scenario occurs comparing the two models and the outcrop data for the middle sector of the ramp. The middle ramp setting is dominated by oligophotic facies; the rhodolithic floatsone (RF - in purple) and large lepidocyclinids (LL - in blue). In the TGSim-model, these two lithofacies are interdigitated moving towards the basin (Fig. 11c). Locally the RF is laterally associated with the LR and CM lithofacies. In this, the RF and LL lithofacies pass towards the more distal depositional environment into a fine calcarenite (FC - in brown) (Fig. 11c), that represent aphotic relatively deeper water sedimentation, eventually with few reworked skeletal assemblages from the middle or inner ramp. The SISim-based model was not able to reproduce these lateral facies heterogeneities, but it reproduces only a random and patchy distribution of the facies association as a coloured like-mosaic (Fig. 12a-c). For example, in the 3D model reproduce by SISim is quite hard to recognise the coral-mound geometry of the CM lithofacies and its geometrical relationships with the SG and LR ltihofacies, as well as with the RF lithofacies, as shown in the depositional model of Fig. 2 and Fig. 13b. Also looking at the distribution of the seagrass lithofacies (in green), in the SISim, seems that this lithofacies can occur throughout the ramp and not only in the inner sector as shown by the TGSim and the model of Pomar et al. (2014). The same observation can easily made for the LL lithofacies (in blue) and the RF lithofacies that in the SISim appear as covering all the study area from the inner to distal zone, whereas the real distribution of that lithofacies occur in the middle sector of the ramp as shown by the depositional model of Pomar et al. (2014) and TGSim.

This comparison between digital data and outcrop data shows that TGSim provides a good match between 3D facies model and observed data, whereas SISim seems to be not so geologically reliable.

5.2. Interpretation of stratigraphic architecture from the digital model

The digital outcrop model allows characterization of the stratigraphic architecture in a fixed spatial framework, providing the basis for additional interpretation of the general evolution through time of the succession of the Porto Badisco Calcarenite. In general, the succession records two main regressive-transgressive cycles where the transgressive phase is represented by soft backstepping of the oligophotoic facies of middle ramp environment onto the inner ramp facies dominated by seagrass. By reconstructing the continuity of the studied outcrops in the model, the trend of progradation and backstepping is observed (Fig. 14).

The general transgressive and regressive trend recognised in the Porto Badisco correlates with third-order eustatic cycles of Haq et al. (1987) and Hardenbol et al. (1998) within the Chattian-Aquitanian. The Porto Badisco Calcarenite is assigned to the SBZ23 (Shallow Benthic Zone) of Cahuzac & Poignant (1997) based on the occurrence of biostratigraphic marker such as miogypsinoid*, Neorotalia lithothaminica, Neorotalia viennoti, Borelis* and nephrolepidinids. Following these authors, SBZ 23 correlates with the upper part of the Chattian to the base of Aquitanian (27-23 Ma).

A direct correlation to third-order eustatic cycles it is not possible because of the use of different biostratigraphic frameworks, different time scales and/or disturbance of the eustatic signal by local tectonism. Nevertheless, there is good correspondence between the first regressive phase recorded by the Porto Badisco succession and the highstand of the Ch2 sequence and the following lowstand. Successive backstepping and progradation coincides with the transgressive highstand of the Ch3 sequence. The final backstepping corresponds to the transgressive phase of the Ch4/Aq1 sequence seen in the sea-level curves of Haq et al. (1987) and Hardenbol et al. (1998). In the investigated succession, there is no evidence of subaerial erosion that would indicate a major sea-level lowstand at the time of formation of the sequence boundaries of the

recognised depositional sequences. The sequence boundary is expressed only as basinward shift of facies belts.

5.3. Influence of the algorithm-type choice on the facies modeling

In the facies modeling the algorithm choice plays a fundamental role in populating the facies distribution (Falivene et al., 2006; Bastante et al., 2008; Amour et al., 2012, 2013). The fit of the algorithm depends also on the classification scale (e.g. lithofacies classification, facies classification) because somehow the classification can simplify in higher or lower degree the real variability of the geological object to model because they are characterised by different functioning modes influencing the facies association and distribution of digital models (Amour et al. 2012; Matheron et al., 1987; Gomez-Hermandez and Srivastava, 1990). The main advantages are the flexibility of the algorithms in populating the cells of the 3D model combining hard and soft data. However, some disadvantages such as the lack of geological reliability have to be considered during the model processing, together with the over- and the under-estimations of the facies distribution. In our study, although the choice of cell size and the input data for the model building is the same, when comparing the SISim and TGSim algorithms, they generate different models. TGSim seems to better honour the complex facies heterogeneity displayed in the Porto Badisco ramp because it transforms the coded facies (e.g. SG, LR, RF, etc.) into a property. This property is partitioned through a numerical threshold (Matheron et al., 1987), which produce transitions between the facies following a trend (for instance, reproducing the transition between the inner ramp facies to the middle ramp facies) along the depositional profile. Also at the scale of depositional geometries, the TGSim seems to be able to reproduce the geometry of geological bodies and the order-trend facies transitions throughout the ramp. For example, the geometry of the CM lithofacies is accurately reproduced in the model with the lens-type geometry of the coral-mound. The capacity of the TGSim in reproducing the depositional geometries and trending of

lithofacies is a powerful tool that provide coherence to both geological concepts (in our case, Walther's law) and interpretations and descriptions derived from field observation, which cannot be handled by the other algorithms like SISim. SISim assigns a facies code pixel-by-pixel by using a local probability distribution that is totally independent from trends, order or lateral association, resulting in more flexibility in producing a layer-cake or mosaic-like facies models but is less useful in modeling at the facies association scale along a depositional profile. The dependence of results on algorithm choice during facies modeling was also described by Tomas et al. (2010) for facies modeling of the Burdigalian Sedini Limestone unit in the Perfugas Basin (Sardinia) or by Amour et al. (2012, 2013) for a Jurassic carbonate ramp of the Central High Atlas in Morocco, or by San Miguel et al. 2013 for a Kimmeridgian coral rich-carbonate ramp of eastern Spain. In these papers, the authors show how the final 3D model reproduced quite faithfully the depositional geometries observed in the outcrops and further elucidates in understanding the relationships between the depositional architecture and facies association transitions. San Miguel et al. (2013) reproduce the Kimmeridgian carbonate ramp in 3D trough two types of models: "full-field model" using the TGSim algorithm and the "sector- model" using the object modeling algorithm. In the first type of model they reproduce in 3D the facies heterogeneity of a carbonate ramp around a relatively large area of 12 Km^2, and instead use the second type of model to characterise the volume of the coral bioconstruction. Amour et al (2012) demonstrated that the TGSim is a good tool for simulating facies transitions within depositional environments for long distances (kilometres to tens of kilometres). The SISim algorithm better works for modeling at lithofacies-scale, that cannot be easily spatially ordered and for vertical facies variation not along a depositional profile. Tomas et al. (2010), choose the SISim algorithm to model the vertical facies relationships during the various stages of platform evolution, but not along the depositional profile. They noted when using the TGSim that the facies variations for the vertical platform evolution are very abrupt. For the Porto

Badisco Calcarenite example is just the opposite because the final 3D facies model demnostrates how the TGSim works better than the SISim. Consequently, during the modeling procedure for carbonate systems the choice of the algorithms is very important and strongly conditioned to the nature of the geological features that have to be modelled as demonstrated both for lateral facies heterogeneity and vertical facies distribution.

6. Conclusions

The Chattian carbonate ramp outcropping in the Porto Badisco area represents a case-study for 3D facies heterogeneity modeling following an ordered proximal-distal trend along the ramp. The excellent quality of the outcrop allows detailed study of the distribution of facies association and architecture along the depositional profile. Combination of field data collection and 3D stochastic workflow by using PETREL^{TM}, have resulted in the generation of a 3D model of facies heterogeneity of the Chattian ramp, which perfectly reproduces the facies transitions from the inner to the outer ramp. The TGSim and SISim stochastic algorithms produce different 3D facies models. Despite the same input data, facies heterogeneity is not well modelled at the facies association scale using SISim because it does not preserve the lateral ordered facies transitions throughout the Porto Badisco ramp. However, the TGSim perfectly reproduces the observed lateral facies heterogeneity along the depositional profile respecting the depositional model of the Porto Badisco carbonate ramp. TGSim is a powerful tool for modeling well-defined spatial facies that follow ordered trend relationships. Three-dimensional modeling represents a useful tool for understanding facies architecture and complex heterogeneity in carbonate systems. In the three-dimensional facies model obtained for Porto Badisco Calcarenite, is it possible to recognised the general evolution through time of the Porto Badisco succession. By reconstructing the continuity of the studied outcrops in the model, the trend of progradation and backstepping is reproduced. The succession records two main regressive-transgressive cycles where the transgressive phase is

represented by soft backstepping of the oligophotoic facies of middle ramp environment onto the inner ramp facies dominated by seagrass. These two phases are correlating with third-order eustatic cycles within the Chattian-Aquitanian interval.

However, the two 3D models presented herein demonstrate how the choice of simulation algorithm is important and related to the capability of the modeler and the scale geological context being modelled. Even if the data inputs are the same the final model can be different.

Acknowledgements

Financial support for this work is provided for Laura Tomassetti by IAS-Post Doctoral (Early Career) Grant Autumn Session 2016. Schlumberger Italiana S.p.A is thanked for academic license of PETREL software. James Hodson (RPS Group) is thanked for English revision. Beatriz Bádenas and an anonymous reviewer are much thanked for their constructive and useful comments that highly improve the quality of the manuscript. Alessandro Romi (Schlumberger Italiana S.p.A) is thanked for his useful advice about using Petrel; Sara Tomás and Hannes Nevermann are thanked for sharing their knowledge about facies modeling.

References

Adams, E.W., Grotzinger, J.P., Watters, W.A., Schroder, S., McCormick, D.S., Al-Siyabi, H.A., 2005. Digital characterization of thrombolite stromatolitereef distribution in a carbonate ramp system (terminal Proterozoic, Nama Group, Namibia). AAPG Bull 89:1293–1318.

Aigner, T., Braun, S., Palermo, D., Blendinger, W., 2007. 3D geological modeling of a carbonate shoal complex: Reservoir analogue study using outcrop data: First Break, v. 25, p. 65–72.

Amour, F., Mutti, M., Christ, N., Immenhauser, A., Agar, S.M., Benson, G.S., Tomas, S., Always, R., Kabiri, L., 2012. Capturing and modeling metre-scale spatial facies heterogeneity in a Jurassic ramp setting (Central High Atlas, Morocco). Sedimentology 59, 1158–1189.

Amour, F., Mutti, M., Christ, N., Immenhauser, A., Benson, G.S., Agar, S.M., Tomás, S., Kabiri, L., 2013. Outcrop analog for an oolitic carbonate ramp reservoir: A scale-dependent geologic modeling approach based on stratigraphic hierarchy. AAPG Bulletin, v. 97, no. 5 (May 2013), pp. 845–871. DOI:10.1306/10231212039.

Bernoulli, D., 2001. Mesozoic–tertiary carbonate platforms, slopes and basins of the external Apennines and Sicily. In: Vai, G.B., Martini, I.P. (Eds.), Anatomy of an Orogen: the Apennines and adjacent Mediterranean basins. Kluwer Acad. Publishers, pp. 307–325

Blendinger, W., Brack, P., Norborg, A.K., and Wulff-Pedersen, E., 2004. Three-dimensional modeling of an isolated carbonate buildup (Triassic, Dolomites, Italy). Sedimentology, 51, 297-314.

Borgomano, J.R.F., Fournier, F., Viseur, S., Rijkels, L., 2008,.Stratigraphic well correlations for 3-D static modeling of carbonate reservoirs: AAPG Bulletin, v. 92,p. 789–824, doi:10.1306/02210807078.

Bosellini, A., Bosellini, F.R., Colalongo, M.L., Parente, M., Russo, A., Vescogni, A., 1999. Stratigraphic architecture of the Salento coast from Capo d'Otranto to S. Maria di Leuca (Apulia, Southern Italy). Riv. Ital. Paleontol. Stratigr. 105, 397–416.

Bosellini, A., Parente, M., 1994. The Apulia Platform margin in the Salento Peninsula (southern Italy). Giorn. Geol. 56, 167–177.

Bosellini, F.R., 2006. Biotic changes and their control on Oligocene–Miocene reefs: a case study from the Apulia Platform margin (southern Italy). Palaeogeogr. Palaeoclimatol. Palaeoecol. 241, 393–409. http://dx.doi.org/10.1016/j.palaeo.2006.04.001.

Bosellini, F.R., Russo, A., 1992. Stratigraphy and facies of an Oligocene fringing reef (Castro Limestone, Salento Peninsula, southern Italy). Facies 26, 146–166. http://dx.doi.org/10.1007/BF02539798

Bosence, D.W.J., Cross, N.E., Hardy, S., 1998. Architecture and depositional sequences of Tertiary fault-block carbonate platforms; an analysis from outcrop and computer modeling. Mar Petrol Geol 15:203–211

Brandano, M., Frezza, V., Tomassetti, L., Pedley, M., Matteucci, R., 2009a. Facies analysis and palaeoenvironmental interpretation of the Late Oligocene Attard member (Lower Coralline Limestone Formation), Malta. Sedimentology 56, 1138–1158.

Brandano, M., Frezza, V., Tomassetti, L., Cuffaro, M., 2009b. Heterozoan carbonates in oligotrophic tropicalwaters: the Attardmember of the lower coralline limestone formation (Upper Oligocene, Malta). Palaeogeography Palaeoclimatology Palaeoecology274, 54–63.

Brandano, M., Morsilli, M., Parente, M., Vannucci, G., Bosellini, F.R., Mateu-Vicens, G., 2010. Rhodolith-rich lithofacies of the Porto Badisco Calcarenite (Upper Chattian, Salento, Apulia, southern Italy). Ital. J. Geosci. 129, 119–131. http://dx.doi.org/10.3301/IJG.2009.10.

Buxton, M.W.N. and Pedley, H.M., 1989. A standardized model for Tethyan Tertiary carbonate ramps. J. Geol. Soc. London, 146, 746–748.

Cahuzac, B., Poignant, A., 1997. Essai de biozonation de l'Oligo-Miocène dans les bassins européens à l'aide des grands foraminifères néritiques. Bull. Soc. Géol. France 168, 155–169.

Deutsch, C. V., Journel, A. G. 1998, GSLIB: Geostatistical software library and user's guide, 2d ed.: Oxford, Oxford University Press, 350 p.

Falivene, O., Arbues, P., Gardiner, A., Pickup, G., Munoz, J.A. and Cabrera, L., 2006. Best practice stochastic facies modeling from a channel-fill turbidite sandstone analog (the Quarry outcrop, Eocene Ainsa basin, northeast Spain. AAPG Bull., 90, 1003–1029.

Falivene, O., Cabrera, L., Munoz, J.A., Arbues, P., Fernandez, O. and Saez, A., 2007. Statistical grid-based facies reconstruction and modeling for sedimentary bodies. Alluvial palustrine and turbiditic examples. Geol. Acta, 5, 199–230.

Galli, A., Beucher, H., Le Loc'h, G., Doligez, B., and Group, H., 1994. The pros and cons of the truncated gaussian method. In Geostatistical Simulations (Eds. M. Amstrong, and P.A. Dowd). Kluwer Acad., Dordrecht, 217–233.

Gómez-Hermández, J., Srivastava, R.M., 1990. ISIM 3D: an ANSI-C three-dimensional and multiple indicator conditional simulation program. Comput. Geosci., 16, 355–410.

Guardiano, F.B., Srivastava, R.M., 1993. Multivariate geostatistics: beyond bivariate moments. In: Soares A. (eds) Geostatistics Tróia '92. Quantitative Geology and Geostatistics, vol 5. Springer, Dordrecht; doi: https://doi.org/10.1007/978-94-011-1739-5_12.

Haq, B.U., Hardenbol J., Vail, P., 1987. Mesozoic and Cenozoic chronostratigraphy and cycles of sea-level change. In: Sea-Level Changes—An Integrated Approach, SEPM Special Publication No. 42 Tulsa, ISBN 0-918985-74-9

Hardenbol, J., Thierry, J., Farley, M.B., Jacquin, T., de Graciansky, P.C., Vail, P.R., 1998. Mesozoic and Cenozoic sequence chronostratigraphic chart. In: Graciansky, P.C., Hardenbol, J., Jacquin, T., Vail, P.R. (Eds.), Mesozoic and Cenozoic Sequence Stratigraphy of European Basins. SEPM Special Publication, 60. SEPM Society for Sedimentary Geology, Tulsa (Chart 1).

Janson, X., Madriz D.D., 2012. Geomodeling of carbonate mounds using two-point and multipoint statistics. Geological Society, London, Special Publications 370, 1, 229-246.

Journel, A.G., Gundeso, R., Gringarten, E. and Yao, T., 1998. Stochastic modeling of a fluvial reservoir: a comparative review of algorithms. J. Petrol. Sci. Eng., 21, 95–121.

Kenter, J., M. Harris, and A. Pierre, 2008. Digital outcrop models of carbonate platform and ramp systems: Analogs for reservoir characterization and modeling (abs.): AAPG International

Conference and Exhibition, Cape Town, South Africa, October 26–29, 2008: http://www.searchanddiscovery.com/documents/2008/08221kenter/ (accessed December 14, 2012).

Kenter, J., M. Harris, and A. Pierre, 2008. Digital outcrop models of carbonate platform and ramp systems: Analogs for reservoir characterization and modeling (abs.): AAPG International Conference and Exhibition, Cape Town, South Africa, October 26–29, 2008: http://www.searchanddiscovery.com/documents/2008/08221kenter/(accessed December 14, 2012).

Kjonsvik, D., Doyle, J., Jacobsen, T., Jones, A., 1994. The effect of sedimentary heterogeneities on production from shallow marine reservoir: What really matters?: Society of Petroleum Engineers paper 28445, 14 p

Koehrer, B.S., Heymann, C., Prousa, F., Aigner, T., 2010. Multi-scale facies and reservoir quality variations within a dolomite body – outcrop analog study from the Middle Triassic, SW German Basin. Mar. Petrol. Geol., 27, 386–411.

Matheron, G., Beucher, H., de Fouquet, C., Galli, A., Ravenne, C., 1987. Conditional simulation of the geometry of fluvio-deltaic reservoirs. SPE Conf., 27–30 September, 591–599, Dallas.

Palermo, D., Aigner, T., Nardon, S., Blendinger, W., 2010. Three-dimensional facies modeling of carbonate sand bodies: Outcrop analog study in an epicontinental basin (Triassic, southwest Germany): AAPG Bulletin, v. 94, p. 475–512, doi:10.1306/08180908168.

Pomar, L., Mateu-Vicens, G., Morsilli ,M., Brandano, M., 2014. Carbonate ramp evolution during the Late Oligocene (Chattian), Salento Peninsula, southern Italy. Palaeogeography, Palaeoclimatology, Palaeoecology 404 (2014) 109–132

Pöppelreiter, M.C., Balzarini, M.A., Hansen, B., Nelson, R., 2008. Realizing complex carbonate facies, diagenetic and fracture properties with standard reservoir modeling software: Geological Society (London) Special Publication 309, p. 39–49.

Qui, L.,.Carr, T.R, Goldstein, R. H., 2007. Geostatistical three-dimensional modeling of oolite shoals, St. Louis Limestone; southwest Kansas: AAPG Bulletin, v. 91, p. 69–96, doi:10.1306/08090605167.

Riding, R., 2002. Structure and composition of organic reef and carbonate mud mounds: concepts and categories. Earth Science Review 58, 163-231. http://dx.doi.org/10.1016/S0012-8252(01)00089-7.

San Miguel, G., Aurell, M., Bádenas, B., Martinez, V., Caline, B., Pabian-Goyheneche, C., Rolando, J.P., Grasseau, N., 2013. Facies heterogeneity of a Kimmeridgian carbonate ramp (Jabaloyas, eastern Spain): a combined outcrop and 3D geomodeling analysis. Journal of Iberian Geology 39, 2, 233-252, http://dx.doi.org/10.5209/rev_JIGE.2013.v39.n1.41761.

Strebelle, S., 2002, Conditional simulation of complex geological structures using multiple-point geostatistics: Mathematical Geology, v. 34, p. 1–22.

Tolosana-delgado, R., Pawlowsky-Glahn, V., Egozcue, J.-J., 2008. Indicator kriging without order relation violations. Math. Geosci., 40, 327–347.

Tomás S., Zitzmann M., Homann M., Rumpf M., Amour F., Benisek M., Marcano G., Mutti M., Betzler, C., 2010. From ramp to platform: building a 3D model of depositional geometries and facies architectures in transitional carbonates in the Miocene, northern Sardinia. Facies, doi:10.1007/s10347-009-0203-7.

Tomassetti, L., Benedetti, A., Brandano, M., 2016. Middle Eocene seagrass facies fromApennine carbonate platforms (Italy). Sedimentary Geology 335, 136–149; http://dx.doi.org/10.1016/j.sedgeo.2016.02.002

Warlich, G.M., Bosence, D.W.J., Waltham, D.A., 2005. 3D and 4D controls on carbonate depositional systems: a sedimentological and sequence stratigraphic analysis of an attached carbonate platform and atoll (Miocene, Nıjar Basin, SE Spain). Sedimentology 52:369–383

White, C.D., Novakovic, D., Dutton, S.P., Willis, B.J., 2003. A geostatistical model for calcite concretions in sandstone. Math. Geol., 35, 549–575.

Wright, V.P., Burgess, P.M., 2005. The carbonate factory continuum, facies mosaics and microfacies: an appraisal of some of the key concepts underpinning carbonate sedimentology. Facies, 51, 17–23.

Figure Captions

Figure 1. A) Simplified geological map of the Salento Peninsula (ACP=Apulian Carbonate Platform; modified after Pieri et al 1997); B) Detailed location of the southern portion of the Salento Peninsula where the study area is located; C) Map view of the Porto Badisco digital elevation model (DEM; horizontal resolution = 8 m). The Porto Badisco ravine has a N-S trend with a E-W segment on its western side. The location of the eleven measured stratigraphic field logs (red dots) and of the five geological cross-sections (red lines) are shown.

Figure 2. Simplified depositional model of the Chattian Porto Badisco Calcarenite homoclinal carbonate ramp (modified after Pomar et al 2014).

Figure 3. A) 3D visualization of Porto Badisco ravine aerial map spread over the DEM (vertical exaggeration = 3). The 3D visualization shows the location of the eleven measured stratigraphic field logs and the orientation of the geological cross-sections imported in the 3D-model. The 3D-model has been elaborated with the PETREL^{TM} software (Schlumberger trademark). B) Close up view of a portion of the study area showing examples of measured stratigraphic field logs in a 3D view.

Figure 4. Example of two geological cross-sections elaborated in the study area and used in the modelling process. A) Along dip geological cross-sections (vertical exaggeration = 3) passing

through, from North to South, the F, E, D, X stratigraphic logs (see Fig. 1C for cross-section location). B) Along strike geological cross-section (vertical exaggeration = 2) passing through, from West to East, the K and J stratigraphic logs (see Fig. 1C for cross-section location).

Figure 5. Field line-drawing photomosaic showing the lateral facies transitions of the Porto Badisco Calcarenite carbonate ramp, in particular are shown the lateral relationships between the rhodolithic floatstone lithofacies (purple), the large lepidcyclinids lithofacies (blue), the large rotaliids lithofacies (yellow) and the fine calcarenite lithofacies (light brown). This facies belt characterises the lithofacies association of the distal part of inner (euphotic) ramp with the LR lithofacies, to middle (olighopothic) ramp with the RF and LL lithofacies, passing to the outer (aphotic) carbonate ramp with the FC lithofacies..

Figure 6. A) 3D view of input data used to generate the geocellular model. DEM data (www.sit.puglia.it) have been loaded as a mesh of points and subsequently interpolated to generate the topographic surface. Convergent gridder algorithm has been used to interpolate the mesh of points; the grid increment along X and Y direction has been set at 8 m. The bottom of the geocellular grid has been set at 0 m a.s.l., close to the lowest stratigraphic data. The final dimensions of the model are 1000 m (in the N-S direction) and 500 m (in the E-W direction). B) Close-up view of the resulting geocellular model showing in detail the dimensions of 3D cells (8 x 8 x 0.20 m).

Figure 7. A) Stratigraphic logs (in dip direction) measured in the field for investigated area of Porto Badisco showing the six recognised lithofacies. For location of logs see figure 1c and 3a; B) Upscaled logs derived from the upscaling process of PETREL showing the comparison between the field measured logs use as data input (on the left) and the pseudo logs created by the software (on

the right). It is possible to note how the thickness of the lithofacies is not changed during the upscaling process. See text for further discussion.

Figure 8. A) Stratigraphic logs (in strike direction) measured in the field for investigated area of Porto Badisco showing three of the six recognised lithofacies. For location of logs see figure 1c and 3a; B) Upscaled logs derived from the upscaling process of PETREL showing the comparison between the field measured logs use as data input (on the left) and the pseudo logs created by the software (on the right). It is possible to note how the thickness of the lithofacies is not changed during the upscaling process. See text for further discussion.

Figure 9. Photomicrographs of the lithofacies characterising the Porto Badisco Calcarenite carbonate ramp. A) Small benthic foraminifera wackestone-packstone lithofacies (SG). Small benthic foraminifera are mainly represented by porcelaneous forms such as miliolids (Mil) and *Peneroplis* (Pe). Coralline red algae are both articulated (ARa) fragments and non articulated (RA) fragments. Micritized cortoids (Co) also occur. Note the poor sorted muddy texture characteristic of seagrass meadow environment. Scale bar is 1 mm. B) Coral mounds lithofacies (CM) characterized by a Porites colony with a skeletal packstone matrix dominated by small benthic foraminifera such as rotaliid (Rot), miliolid (Mil) and larger benthic foraminifera as *Amphistegina* (Am). Scale bar is 1 mm. C) Large rotaliid packstone lithofacies (LR) dominated by hyaline-perforated foraminifera as rotaliids mainly represented by the genus *Neorotalia* sp. and *Neorotalia viennoti* (RotV) associated with red algae fragments both of articulated (Ara) and non-articulated (RA) and echinoid plates (Ech). Scale bar is 1 mm. D) Rhodolithic floatstone lithofacies (RF) showing laminar to columnar rhodolith growing with an encrusting acervulinid foraminifera (Ac). The skeletal fraction of the matrix is characterised by bryozoans (Bry), echinoids and nummulitid form such as *Heterostegina* (He). Scale bar is 1 mm. E) Large lepidocyclinid packstone(LL) characterised by large specimens of lepidocyclinids (both *Eulepidina* and *Nephrolepidina*) (Lep),

Amphistegina (Am) and *Spiroclypeus* (Sp). Also red algae fragments are present. Scale bar 1 mm. F) Fine calcarenite lithofacies (FC) characterised by a discrete grain sorting, higly abraded, skeletal components, dominated by coralline algal debris, echinoid fragments, small benthic foraminifers and rare nummulitids and lepidocyclinids. Scale bar is 1 mm.

Figure 10. Comparison between field geological cross-sections (see Fig. 4) and pseudo cross-sections exported from the 3D facies model of the Porto Badisco Calcarenite carbonate ramp using TGSim method. The pseudo cross-sections have been exported along the same traces of the field geological cross-sections (see Fig. 1C). A) Along dip field geological cross-section (top) compared with the pseudo geological cross-section (bottom). Note the quite good fit of the lithofacies SG, CM, LR, RF in the left corner of the field cross-section with the one reproduce by the 3D model. Of course some uncertainness can be present. B) Along strike field geological cross-section (top) compared with the pseudo geological cross-section (bottom). Note in the area between the log J and log K how the lateral relationships of the lithofacies LL, FC and RF are reproduce by the model fitting quite well with the geological field cross-section.

Figure 11. A) 3D view of the final facies model of the Porto Badisco Calcarenite carbonate ramp using TGSim (vertical exaggeration = 3). It is possible to observe how the TGSim, by means of constraining tools (i.e., measured stratigraphic field logs and the geological cross-sections), allows to replicate and to model the lithofacies variability trends throughout the depositional profile as described by Pomar et al. (2014(. The 3D view highlights the high heterogeneity degree and the lateral transition of the lithofacies association. B) and C) close up views of the proximal (Fig. 11B) and distal (Fig. 11C) sector of the modelled Porto Badisco Calcarenite carbonate ramp with the TGSim method.

Figure 12. A) 3D view of the facies model of the Porto Badisco Calcarenite carbonate ramp using SISim (vertical exaggeration = 3). The model obtained with the SISim method, compared to the TGSim, does not replicate the lateral facies heterogeneity observed along the depositional profile of the Porto Badisco ravine as described by Pomar et al. (2014). The resulting model is characterised by high degree of randomness. B) and C) close up views of the proximal (Fig. 12B) and distal (Fig. 12C) sector of the modelled Porto Badisco calcarenite ramp with the SISim method.

Figure 13. A) Field-photomosaic showing the lateral facies transitions of the Porto Badisco calcarenite system. Note the mound-like geometry of CM lithofacies and its lateral interfingering with SG and LR lithofacies. B) detailed sketch from the 3D model generated by TGSim algorithm reproducing the lateral interfingering between the CM, LR and SG lithofacies. It is possible to recognised how the TGSim reproduces the mound-like geometry of the CM lithofacies.

Figure 14. 3D view of the facies model obtained with the TGSim method showing the stratigraphic architecture of Porto Badisco Calcarenite carbonate ramp. The obtained digital section of the model (refer to the inset figure for the section location) shows the progradation and backstepping trends of the Porto Badisco calcarenite ramp corresponding to the 3rd order eustatic cycle of Haq et al. (1987) and Hardenbol et al. (1998) for the Chattian-Aquitanian interval.

Figure 1

Click here to download high resolution image

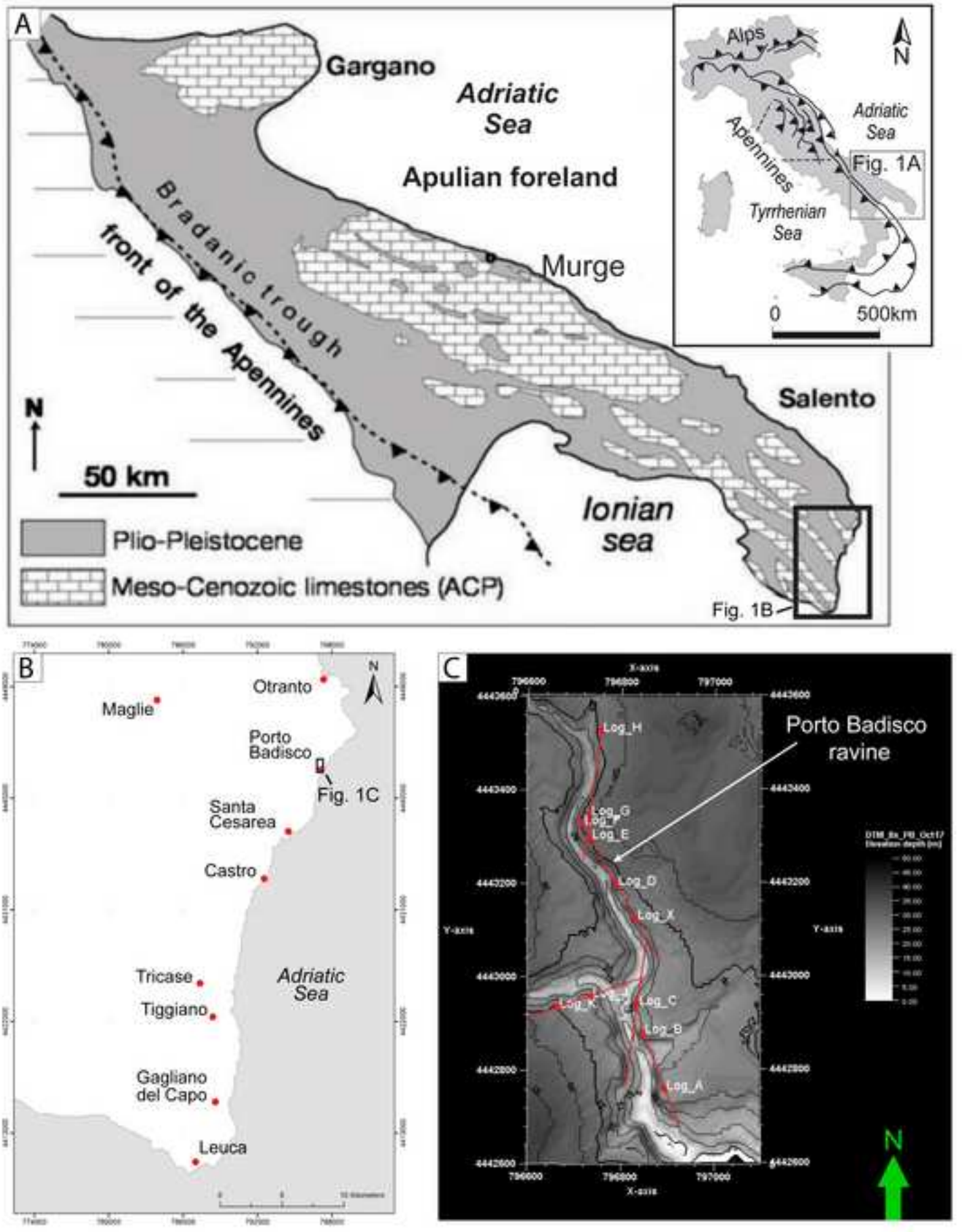

Figure 2

Click here to download high resolution image

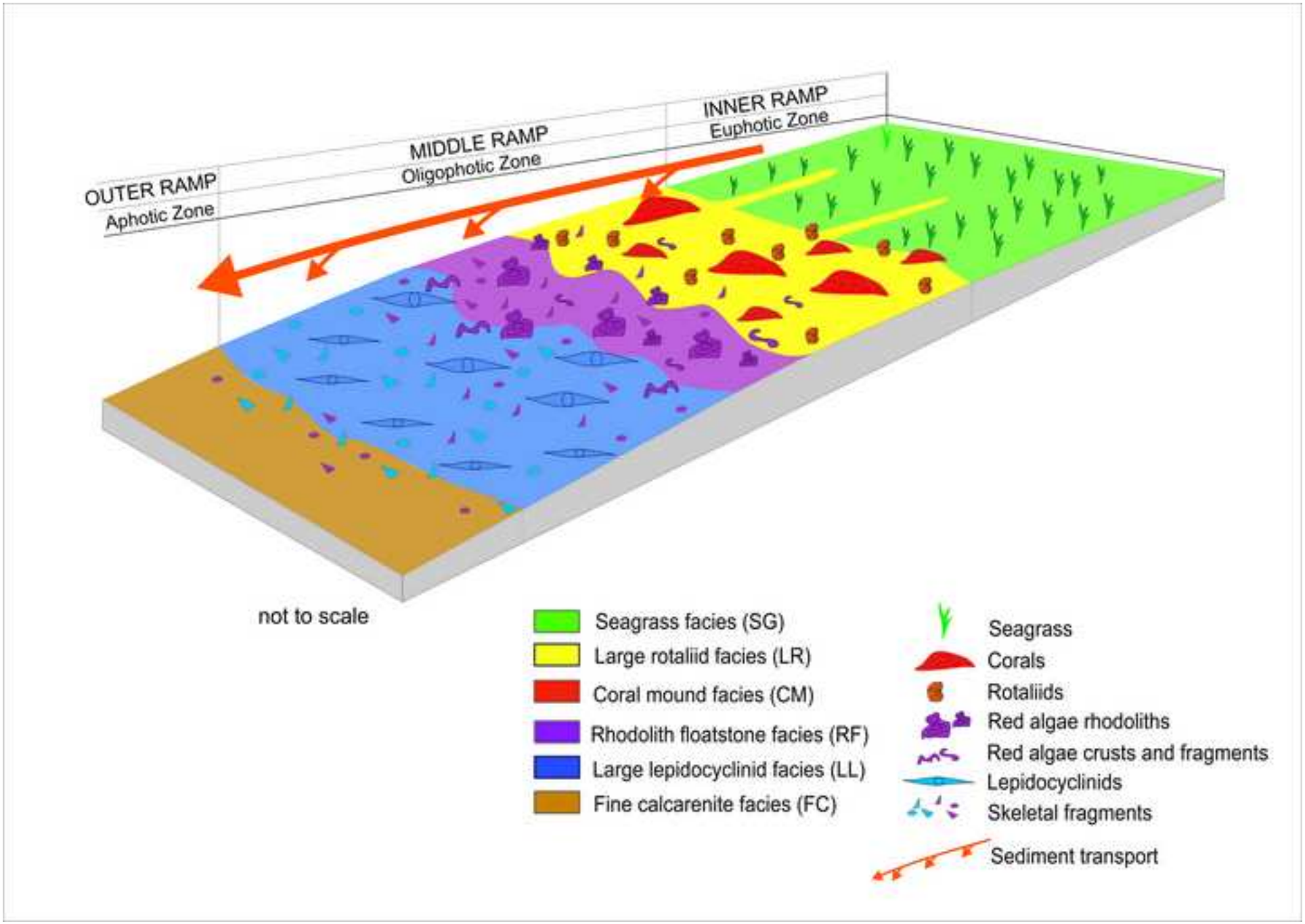

Figure 3

Click here to download high resolution image

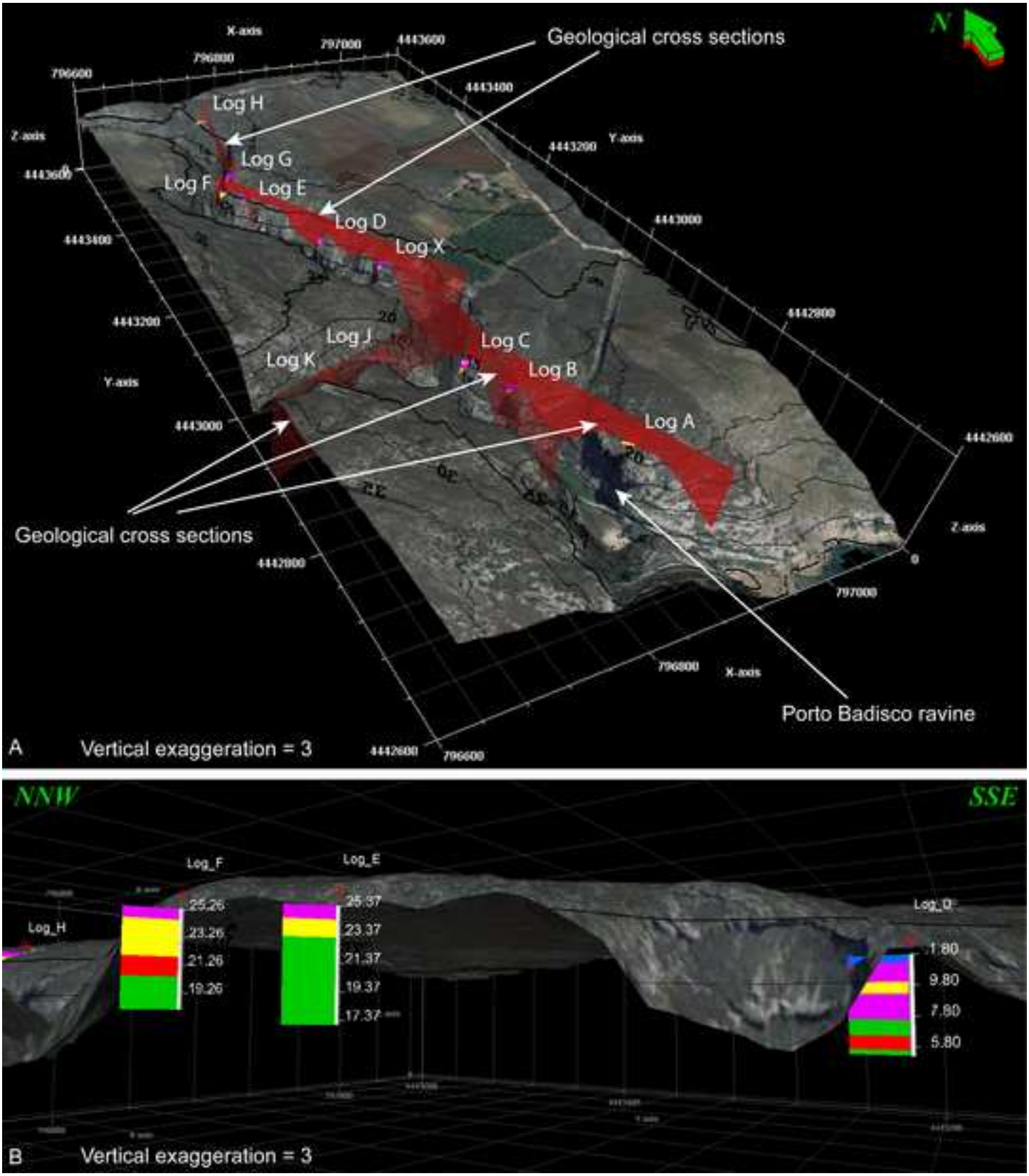

Figure 4

Click here to download high resolution image

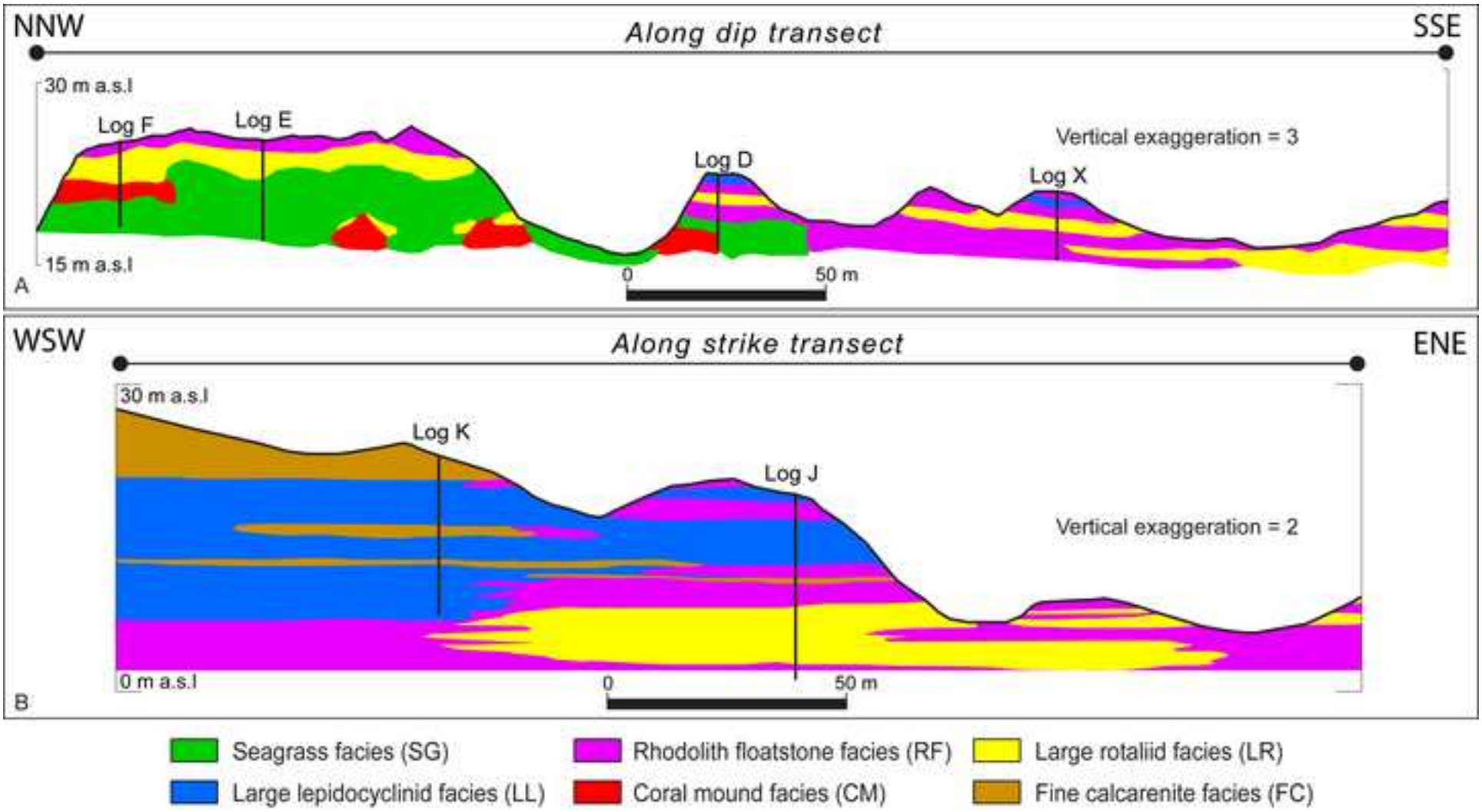

Figure 5

Click here to download high resolution image

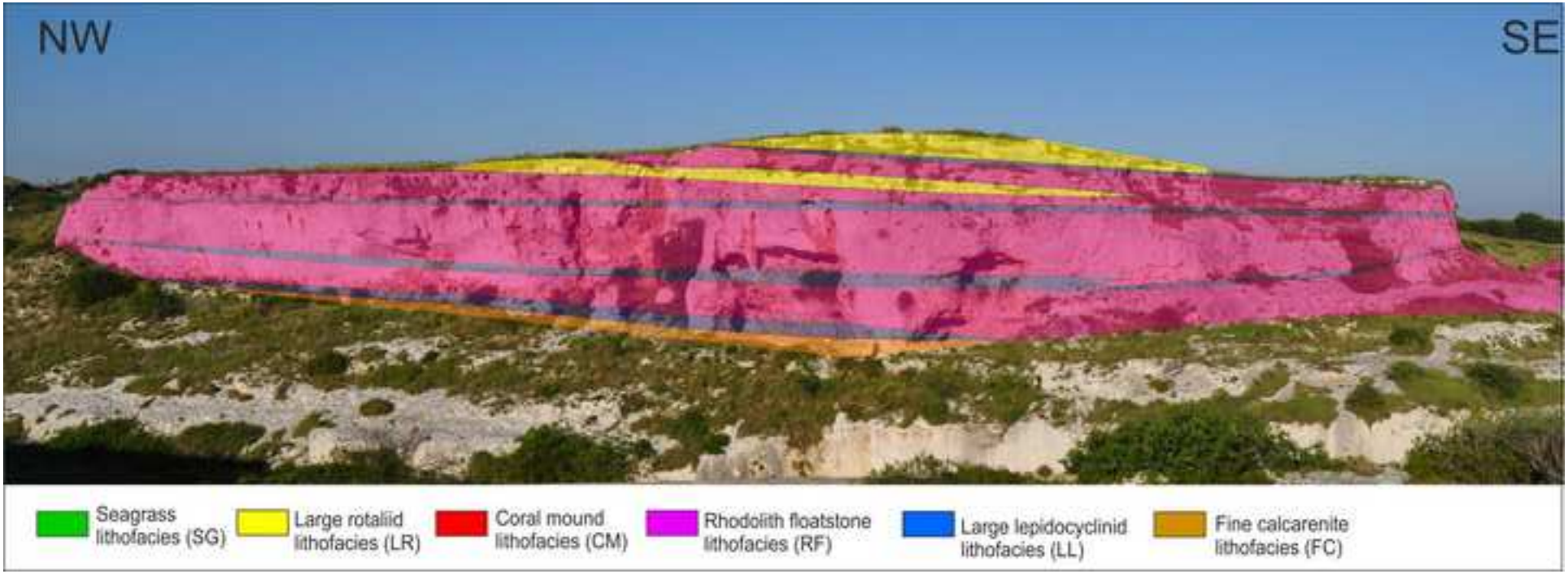

Figure 6

Click here to download high resolution image

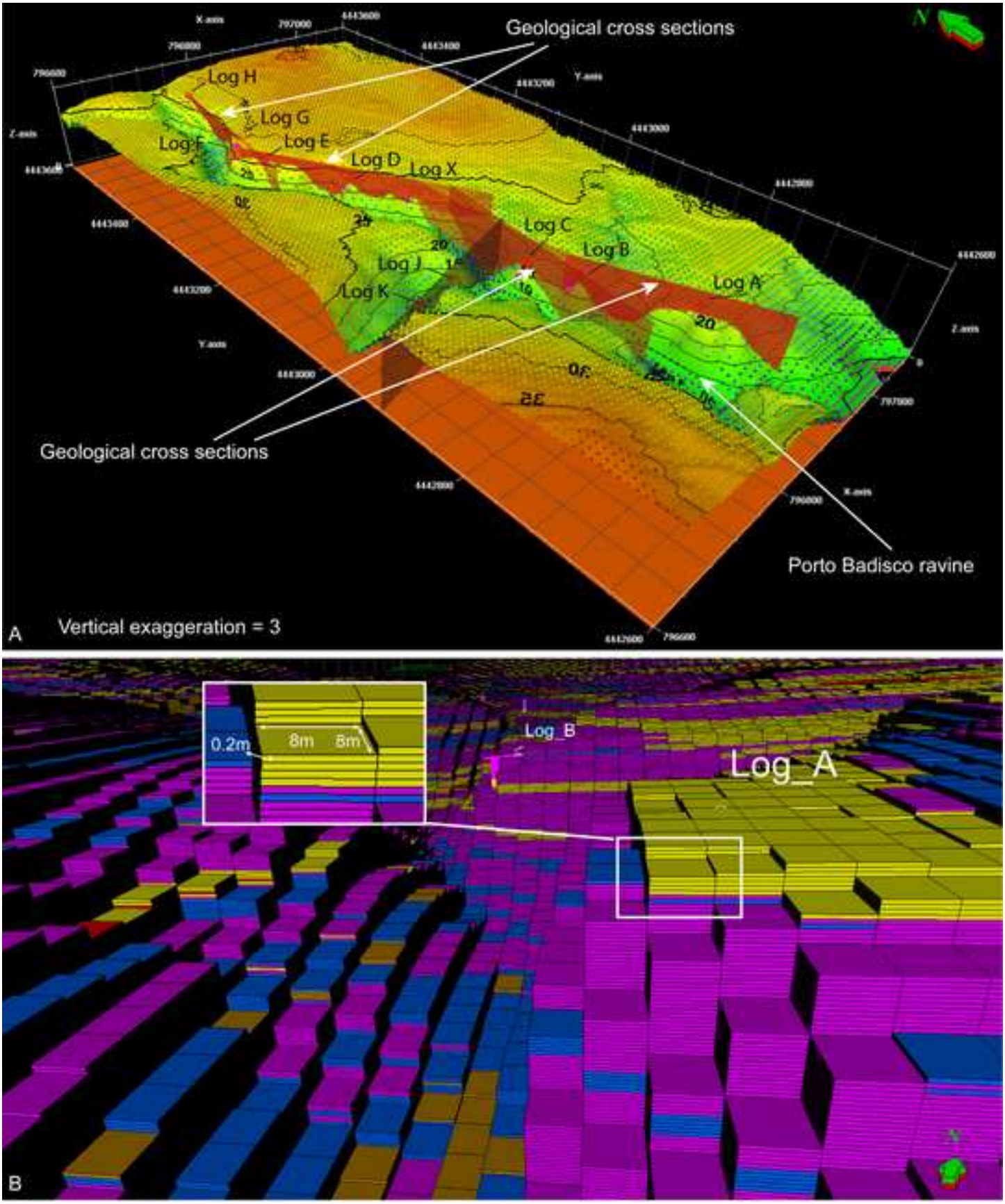

Figure 7

Click here to download high resolution image

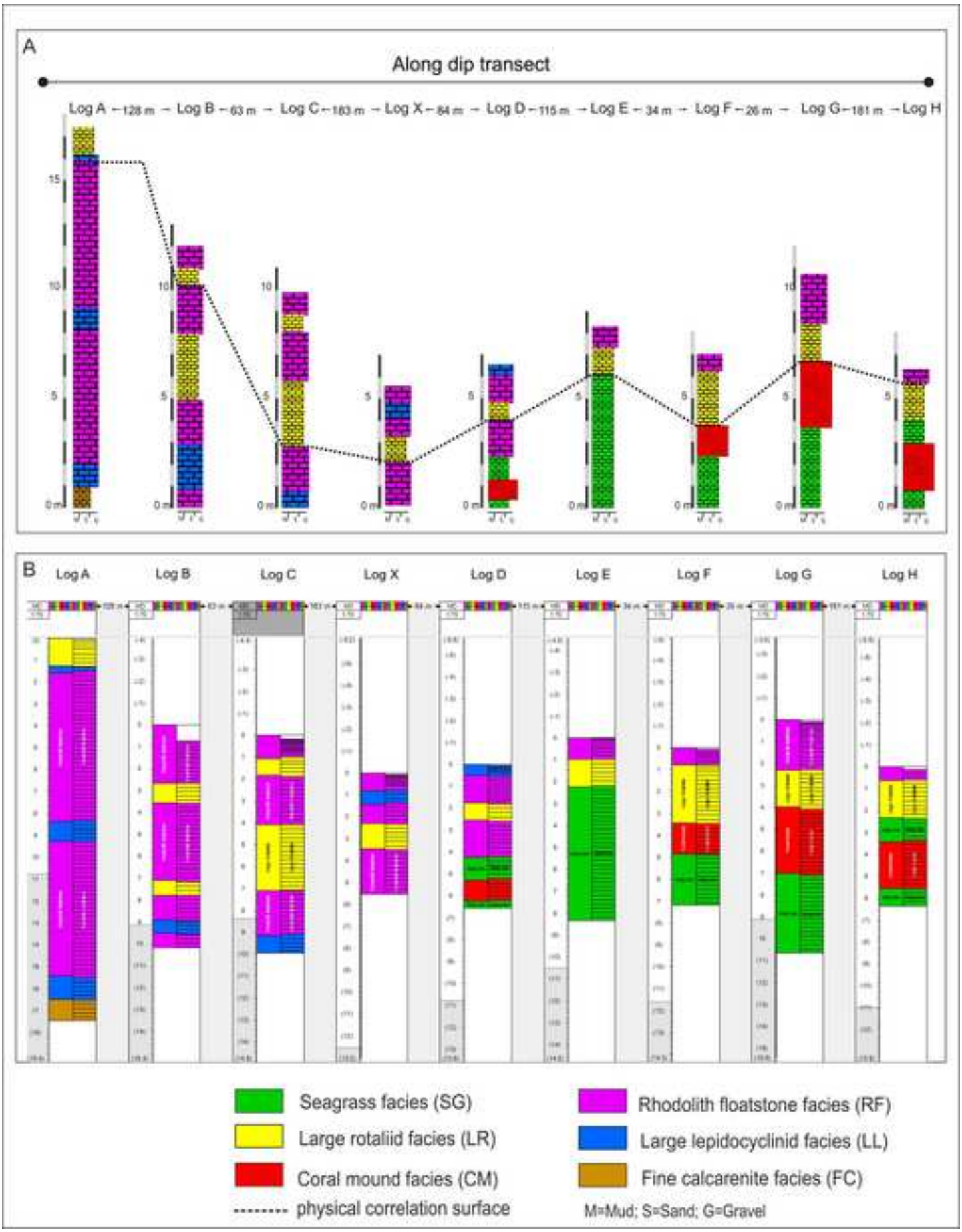

Figure 8

Click here to download high resolution image

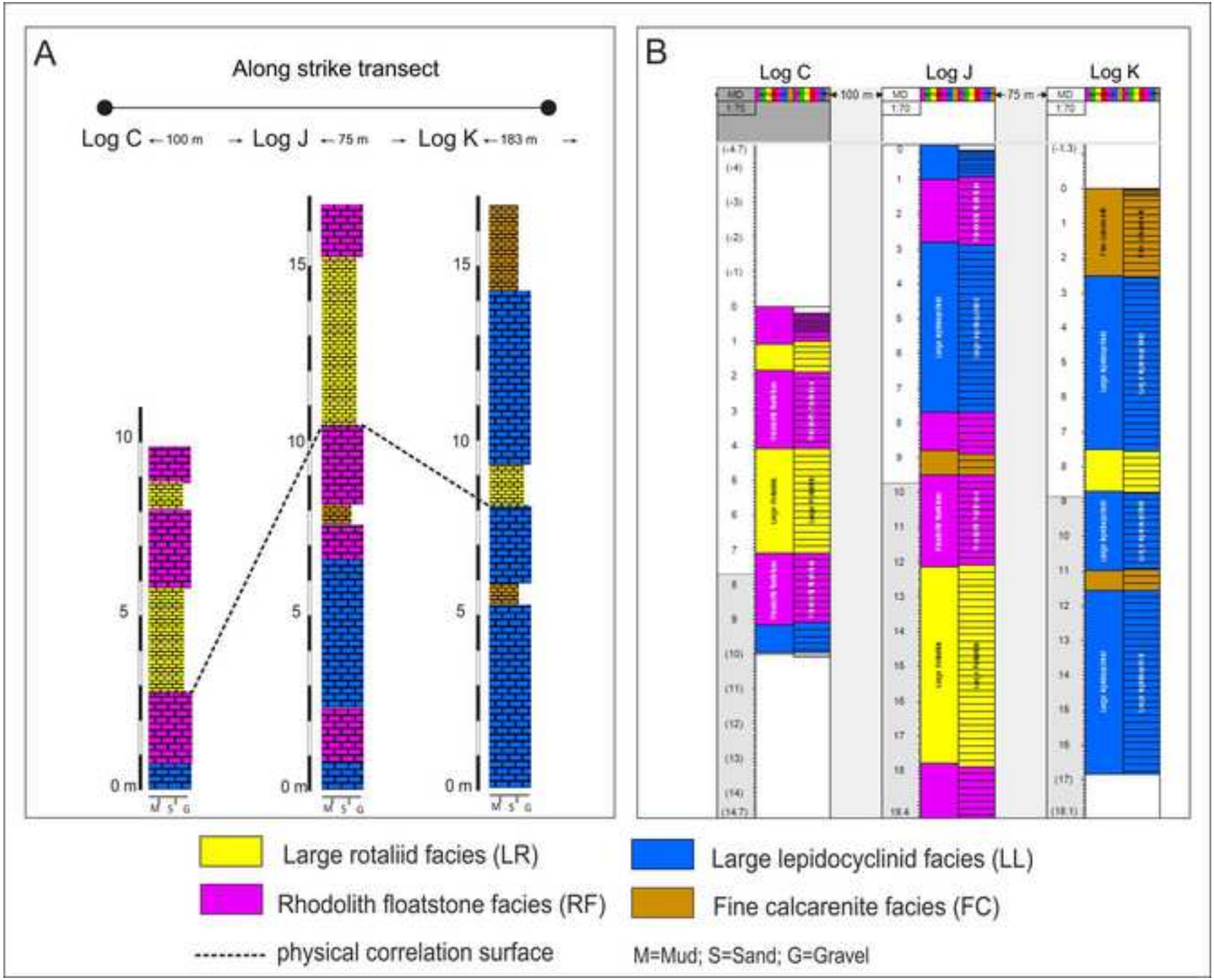

Figure 9
Click here to download high resolution image

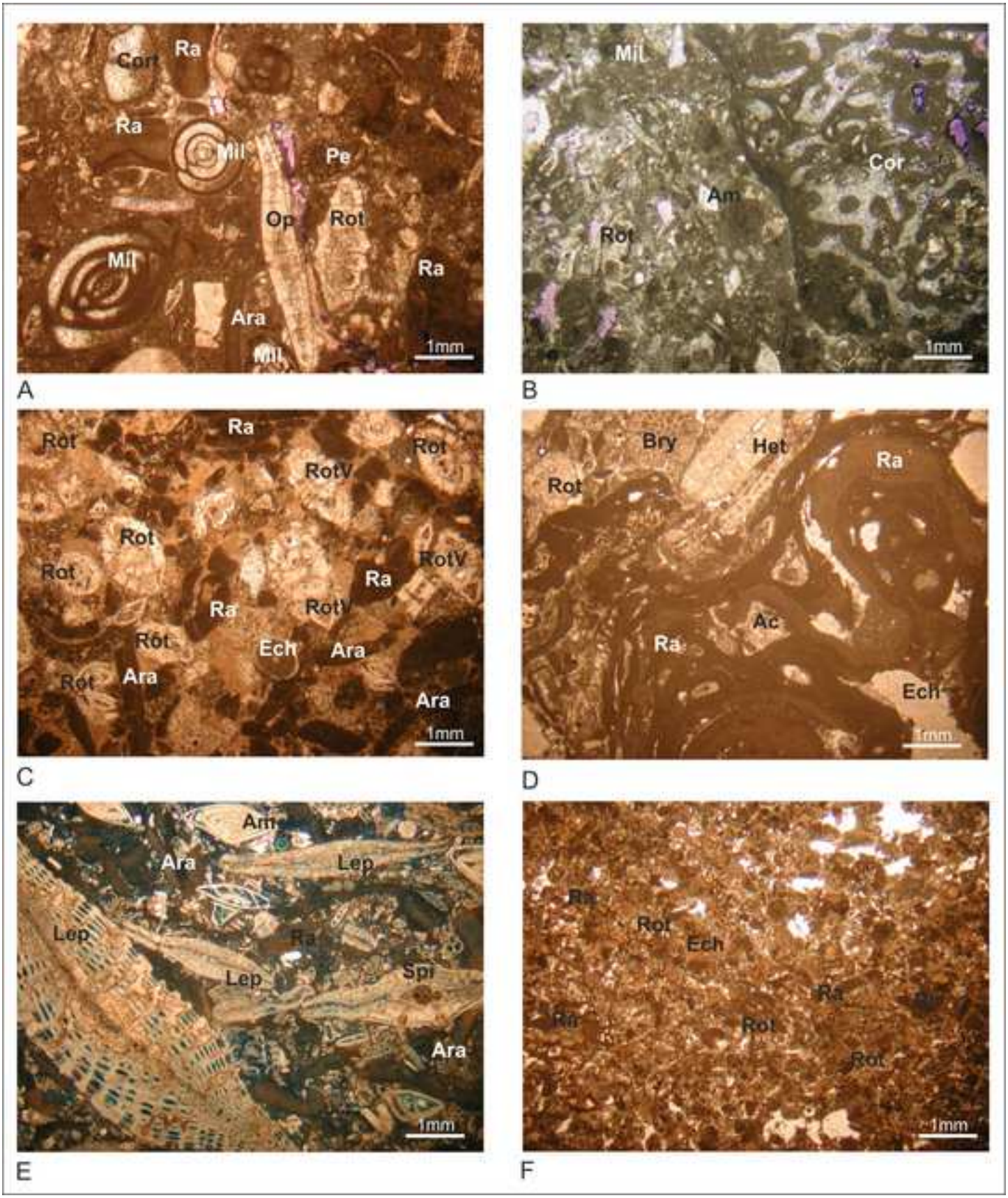

Figure 10

Click here to download high resolution image

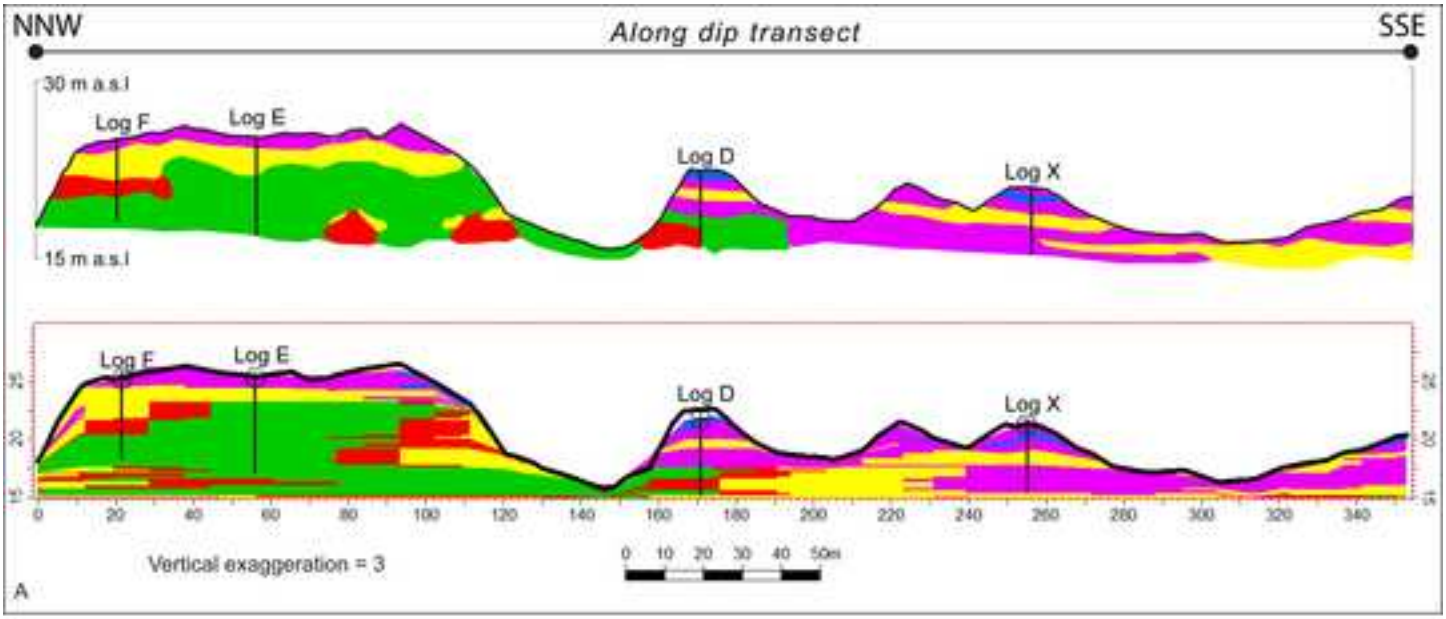

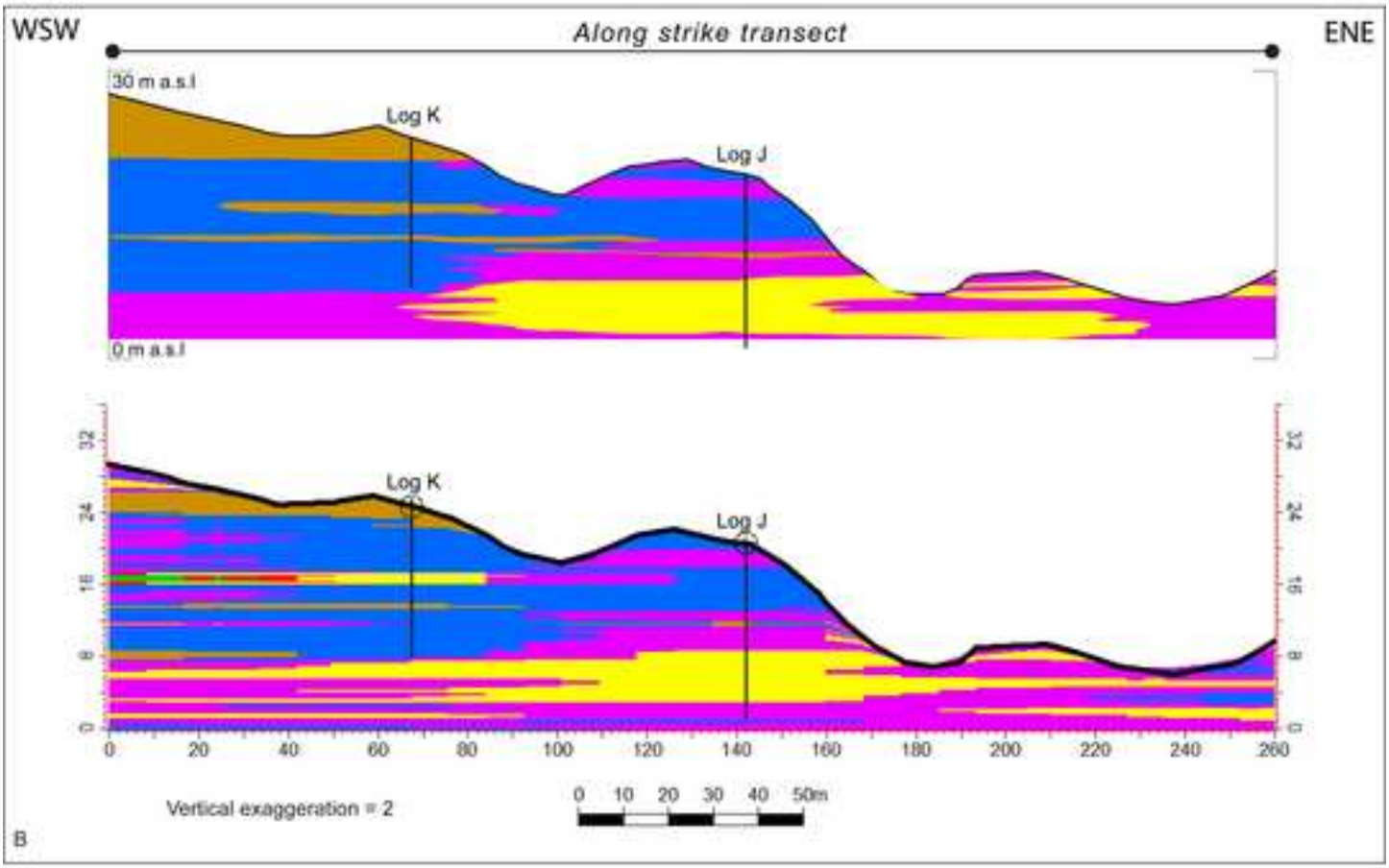

Seagrass facies (SG)
Large lepidocyclinid facies (LL)
Rhodolith floatstone facies (RF)
Coral mound facies (CM)
Large rotaliid facies (LR)
Fine calcarenite facies (FC)

Figure 11

Click here to download high resolution image

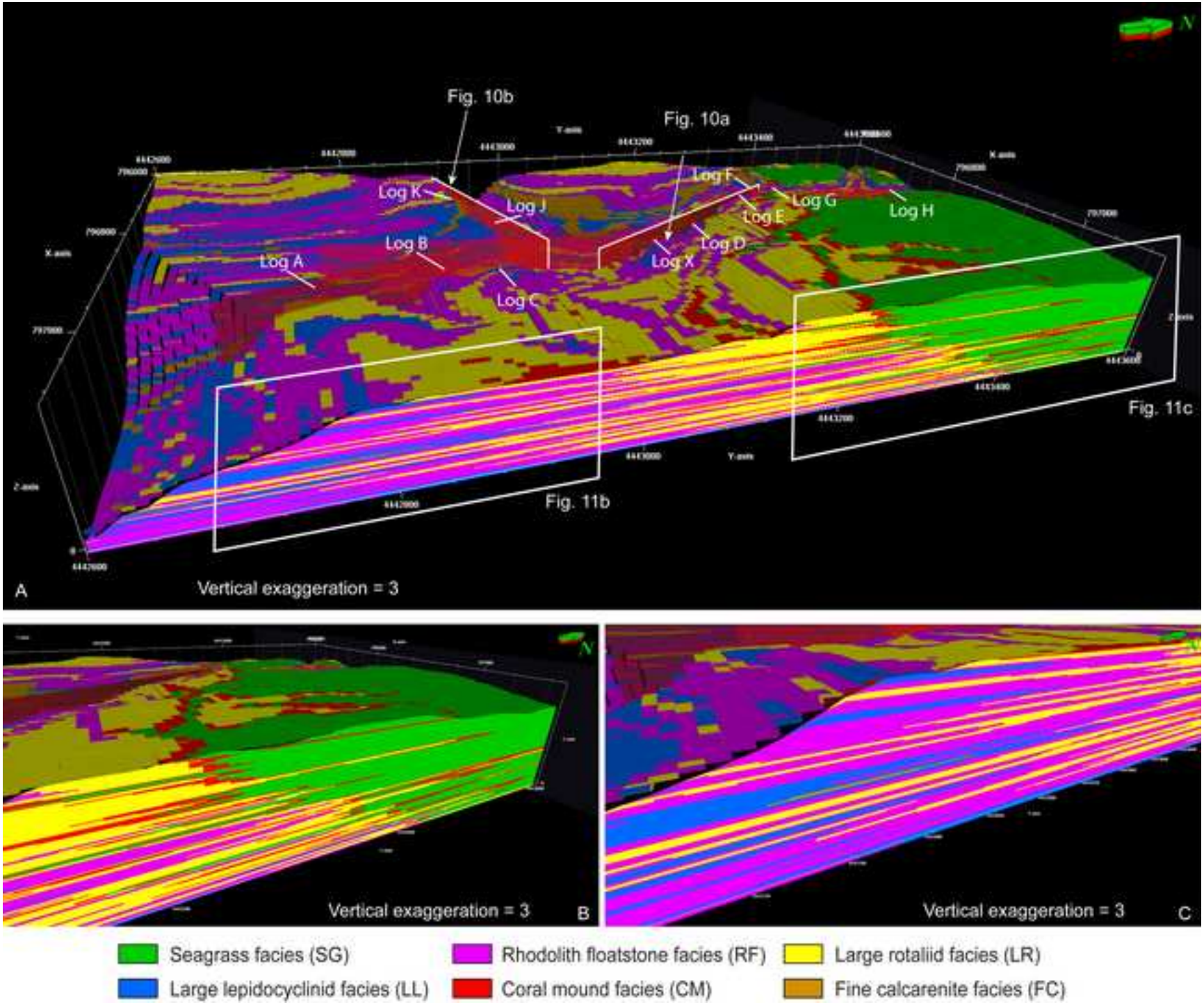

Figure 12

Click here to download high resolution image

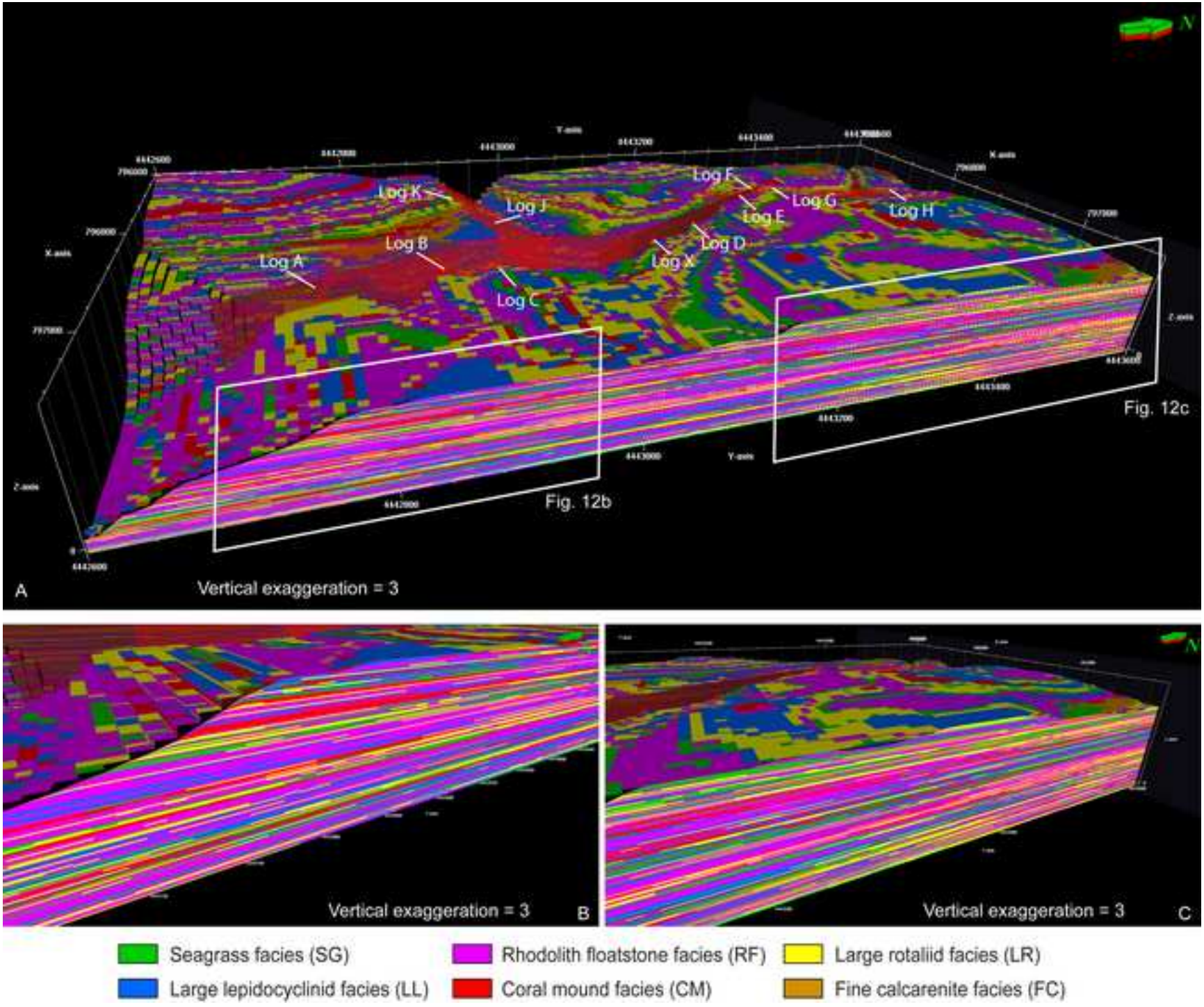

Figure 13

Click here to download high resolution image

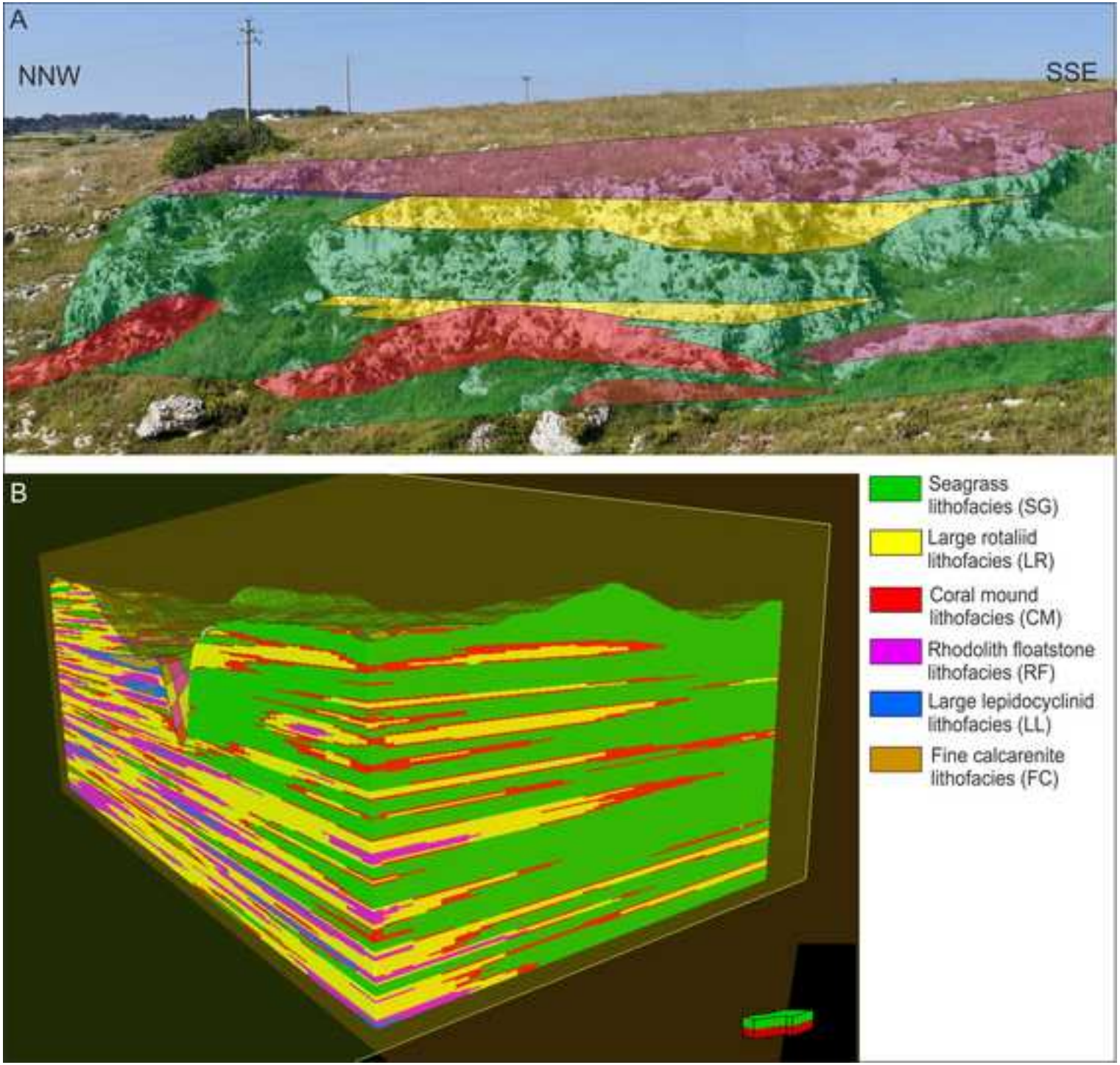

Figure 14

Click here to download high resolution image